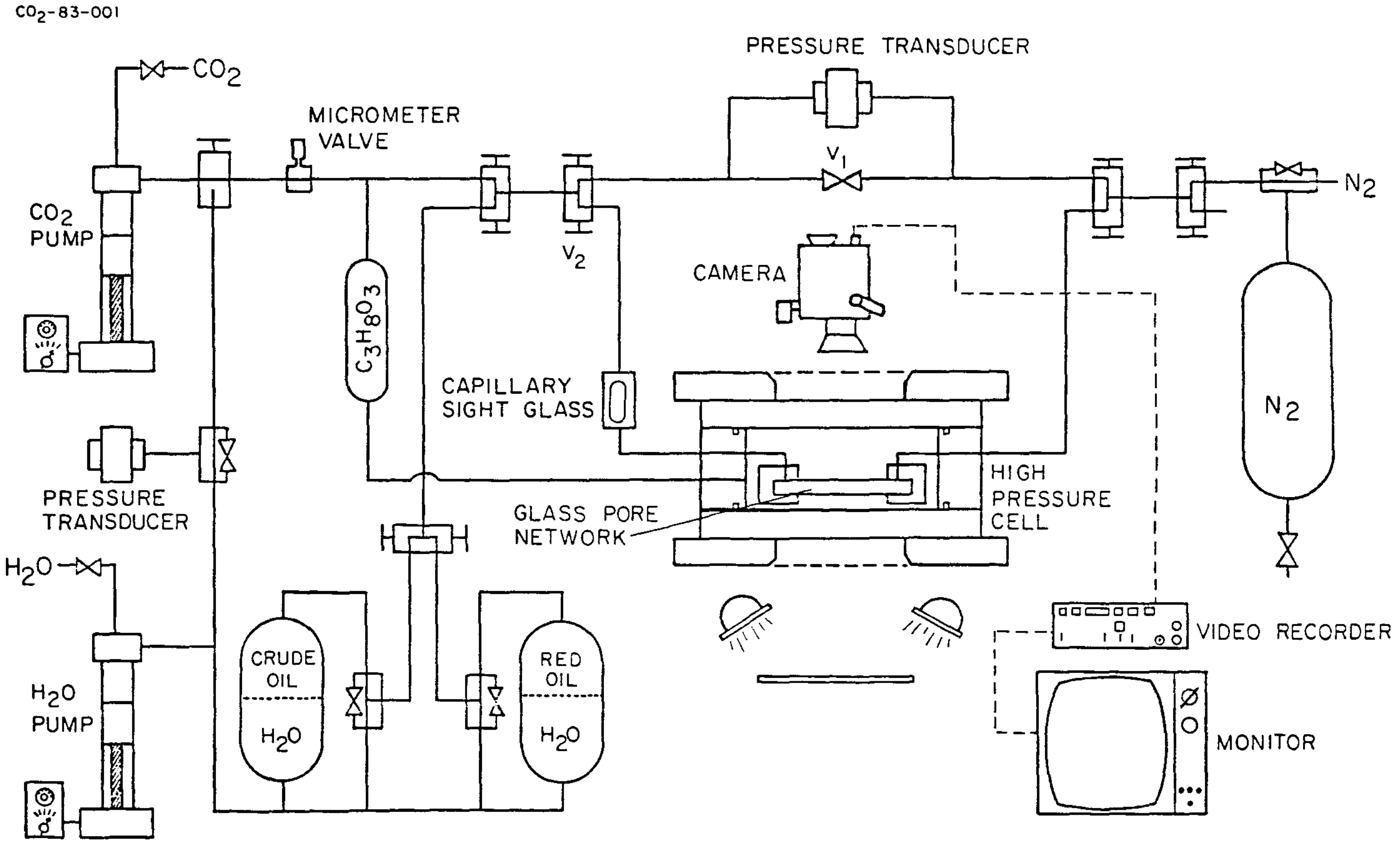
CO2-83-001
CO2
PRESSURE TRANSDUCER
MICROMETER VALVE
V1
N2
CO2 PUMP
V2
CAMERA
C3H8O3
CAPILLARY SIGHT GLASS
N2
PRESSURE TRANSDUCER
HIGH PRESSURE CELL
GLASS PORE NETWORK
H2O
H2O PUMP
CRUDE OIL
H2O
RED OIL
H2O
VIDEO RECORDER
MONITOR

Fig. 3.3 Apparatus for flow visualization experiments.

variations in cell temperature over the course of an experiment could materially alter the actual rate. For instance, if the pump contained 100 cm^3 of CO_2, a temperature change of 0.1°C would cause the total volume of the CO_2 to change by 0.18 $cm,^3$ nearly one PV for some models. Thus, the pore volumes shown for CO_2 and N_2 floods should be taken as indicators of time sequence only.

Between displacements, the flow lines and glass model were cleaned with tetrahydrofuran and an organic solvent (Chem-Solv, Malinckrodt, Inc.), rinsed with water, and then flushed with acetone. The acetone was evaporated with N_2 which was then displaced with CO_2.

3.2 Secondary Displacement Experiments

Three displacements in which water was absent were performed in each pore network:

(1) Displacement of red-dyed Soltrol by blue-dyed Soltrol at 8.3 MPa (1200 psia).

(2) Displacement of red-dyed Soltrol by CO_2 at 8.3 MPa (1200 psia).

(3) Displacement of Maljamar crude oil by CO_2 at 8.3 MPa (1200 psia).

Displacement (1) was intended to identify preferential flow paths in each model with a miscible, unit viscosity ratio flood. The effects of viscous instability in a first contact miscible displacement were examined in (2). Displacement (3) was an unstable, multiple contact miscible flood.

Two additional experiments were performed in micromodel 3:

(4) Displacement of Maljamar crude oil by CO_2 at 5.52 MPa (800 psia).

(5) Displacement of Maljamar crude oil by N_2 at 5.52 MPa (800 psia).

Both displacements were unstable, immiscible floods. They were performed to examine the effect of solubility of the injected fluid in the displaced fluid on displacement performance. Doscher and El-Arabi (1981) suggested, for instance, that oil recovery in tertiary CO_2 floods is strongly influenced by solubility. At the displacement conditions, the solubility of CO_2 in the oil was estimated from PVT experiments (see §2.1) to be about 60 mol %. From PVT data for N_2 and Wasson oil, a very similar Permian basin oil, the solubility of N_2 was estimated to be about 10 mol %. Thus, N_2 was much less soluble at the same conditions.

First Contact Miscible Displacements

Results of displacement (1) for model 3 are shown in Fig. 3.4. Results of the floods in models 1 and 2 were similar and hence are not shown here. Detailed results of all of the floods are reported by Campbell (1983a). In model 1, the flood fronts were quite smooth, as expected for that model of uniform pores. Models 2 and 3 had pores of varying sizes. The resulting heterogeneity caused some irregularity in the flood fronts, as shown in Fig. 3.4. In addition, the geometry of injection and production ports caused faster flow along the center line of the model. Even so, breakthrough occurred at 0.95 PV, and essentially all of the red oil was recovered by about 1.15 PV. Hence, the heterogeneity of the model did not have a large effect on recovery.

The orientation of the pores in models 2 and 3 also slowed recovery of the red oil slightly, as is illustrated in Fig. 3.5 for model 3. Pores which were perpendicular to the local flow direction were not swept. Instead, the red oil diffused slowly into the adjacent flowing streams. Thus, pore orientation with respect to the direction of flow produced effects similar to those of dendritic or dead-end pores, though the model contained no actual dead-end pores.

Fig. 3.6 shows results of the displacement of the red oil by CO_2. In that displacement, the ratio of the viscosity of the oil to that of CO_2 was about 22 (Table 3.1). The resulting viscous instability exaggerated the effects of pore heterogeneity in the model, so that the flood fronts were more irregular, but all of the red oil was eventually recovered by the first contact miscible displacement.

Multiple Contact Miscible Displacements

Fig. 3.7 shows results of the displacement of Maljamar crude oil by CO_2. In that displacement, the viscosity ratio was nearly 50, and hence, the displacement front was significantly more irregular than in the displacement of Soltrol by CO_2. Effects of the phase behavior of the CO_2-oil mixtures could also be seen. Not all of the oil was recovered in this multiple contact miscible displacement, though the amount of residual oil left was quite small. Furthermore, the visual observations confirm that there was an interaction between viscous instability and phase behavior, as predicted by Gardner and Ypma (1982). Fig. 3.8 shows the positions of the CO_2 front just before and just after breakthrough (0.64 PV) along with the location of oil at a later time (0.88 PV). The dark oil-rich phase shown within the boundary of the central finger appeared in the area from which all the oil had been completely removed during the passage of the finger. The oil shown in the corners of the model had not yet been contacted. Flow of oil-rich phase from the edges of the finger to its center was observed. The oil-rich phase appeared to form as oil at the edge of the finger mixed by cross flow with CO_2 in the finger.

The observed behavior was consistent with the idea that the finger contained CO_2 which was not enriched with intermediate hydrocarbons extracted from the oil, so that when it mixed with oil from the edge of the finger, a

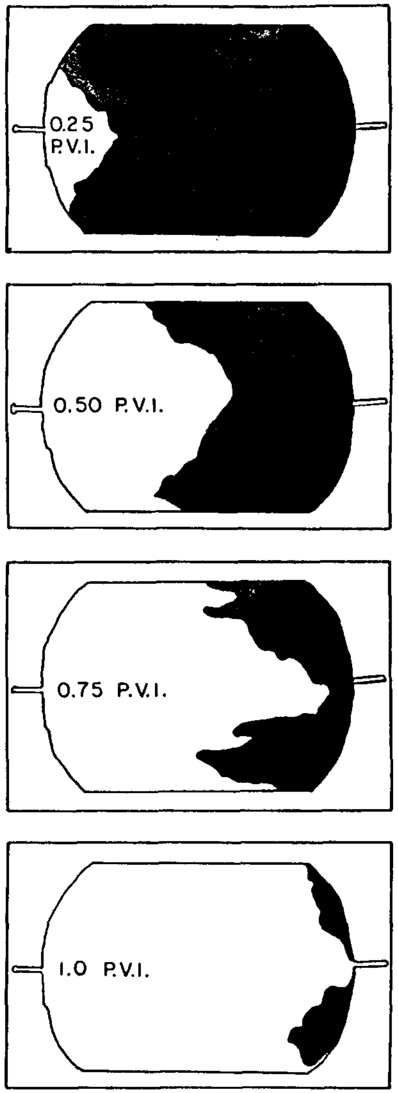
0.25
P.V.I.
0.50 P.V.I.
0.75 P.V.I.
1.0 P.V.I.

Fig. 3.4 Secondary displacement of red-dyed Soltrol by blue-dyed Soltrol in micromodel 3.

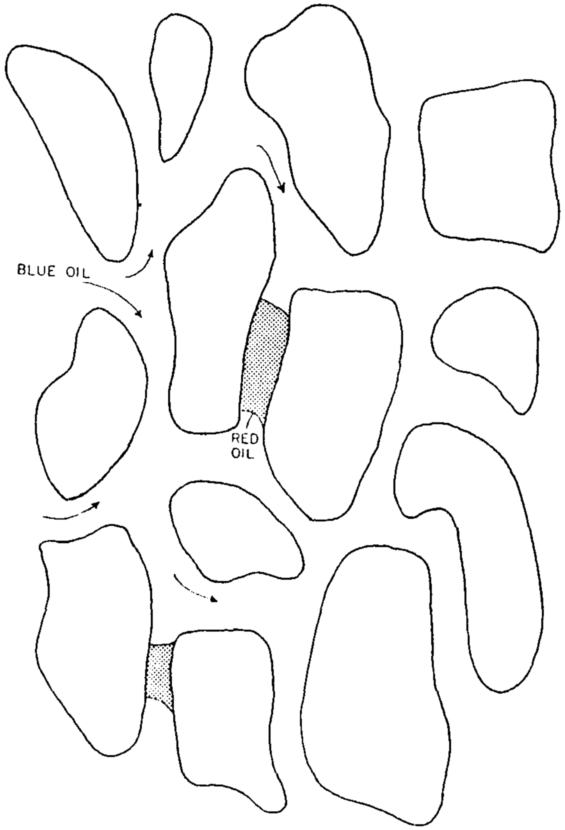
BLUE OIL
RED OIL

Fig. 3.5 Recovery of red Soltrol from pores transverse to the local flow direction.

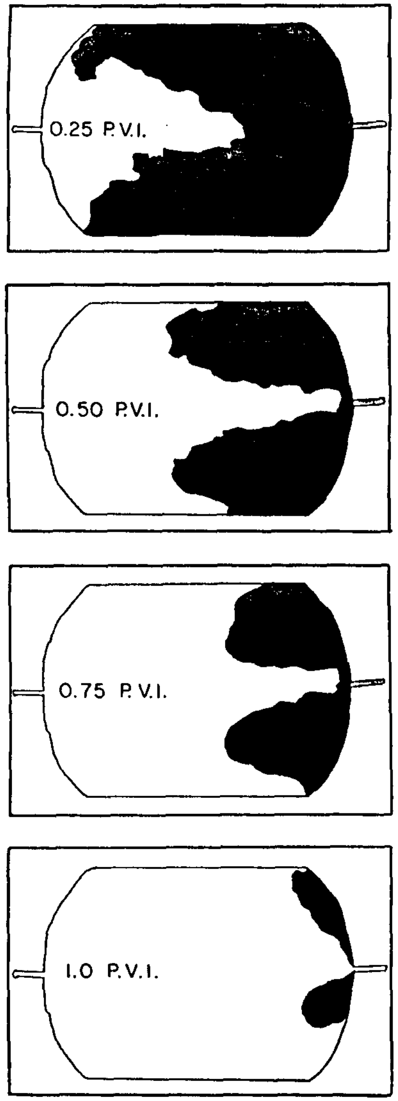
0.25 P.V.I.
0.50 P.V.I.
0.75 P.V.I.
1.0 P.V.I.

Fig. 3.6 Secondary displacement of red Soltrol by CO_2 at 25°C and 8.3 MPa in micromodel 3.

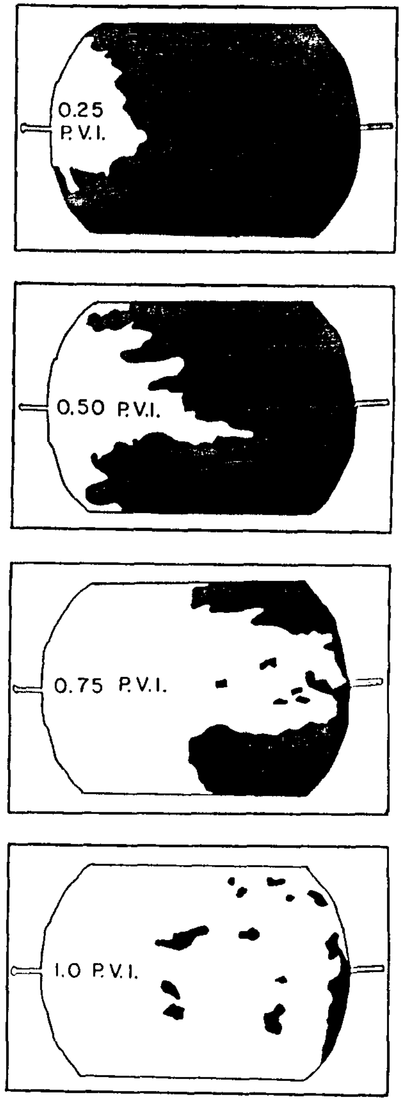
0.25 P.V.I.
0.50 P.V.I.
0.75 P.V.I.
1.0 P.V.I.

Fig. 3.7 Secondary displacement of Maljamar crude oil by CO_2 at 25°C and 8.3 MPa in micromodel 3.

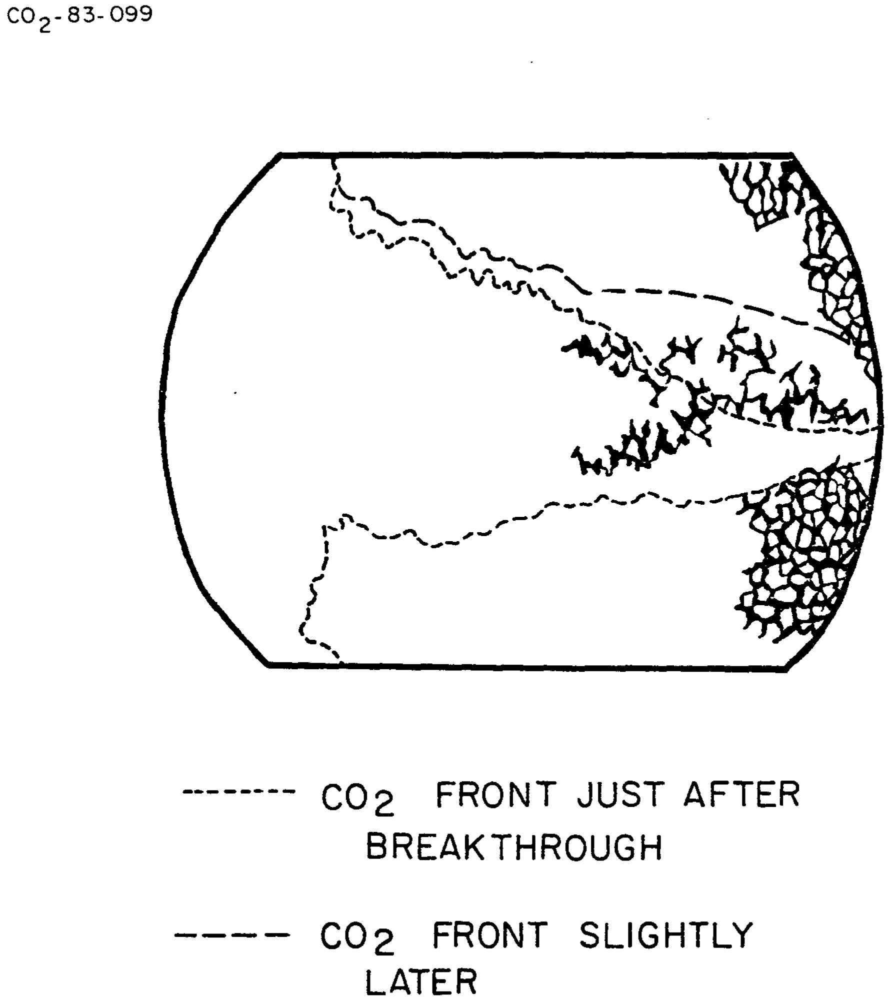
CO_2-83-099
------- CO_2 FRONT JUST AFTER BREAKTHROUGH
---- CO_2 FRONT SLIGHTLY LATER

Fig. 3.8 Appearance of oil-rich phase in the region first penetrated by a viscous finger.

second phase formed (Gardner & Ypma 1982). Simulation results reported by Gardner and Ypma (1982) indicated that viscous cross-flow caused the oil-rich phase to mix with lean CO_2 at the trailing edge of a finger. Fig. 19 of their paper, for instance, describes remarkably well the behavior of the CO_2-crude oil displacements reported here. Gardner and Ypma argued that transverse dispersion could also cause such mixing, but with the relatively high velocities and large pores used here, it seems likely that viscous effects dominated the mixing at the edge of the finger. It is also possible that capillary driven flow in the grooves bounding the pores contributed to mixing of oil with unenriched CO_2 in the finger. In any case, the observations described provide direct evidence that viscous instability interacts with phase behavior. The results reported are completely consistent with the explanation given by Gardner and Ypma of the mechanism of the interaction.

Some of the oil shown within the finger in Fig. 3.8 was subsequently recovered by continued extraction of hydrocarbons by the CO_2 and by some two-phase flow. In fact, the presence of the second phase probably aided recovery by limiting flow in the areas where residual oil was present, thereby directing flow to unswept areas. While relative permeability effects could be expected whenever two phases are present, it seems likely that such effects would be less important in pore networks connected in three dimensions.

It is apparent from Fig. 3.8 that the first half of the model contained less residual oil than the other half. A conventional description of the effects of phase behavior based on mixing cells might suggest the opposite: the residual oil saturation should be higher in the inlet region where the development of miscibility takes place. In the displacements described here, the mixing of CO_2 and oil really began in the flow lines upstream of the model. Thus, a transition zone had already developed by the time CO_2 reached the model. Calculations of the size of the transition zone from Taylor's (1953) analysis, however, suggest that they had volumes of not more than 10-13% of the model volume (see Campbell 1983a for details). Such small transition zones probably lead to high displacement efficiency in the inlet region and somewhat lower efficiency downstream where viscous fingers had penetrated the transition zone, mixing lean CO_2 with uncontacted oil. In that region, the multiple contact process regenerated the enriched CO_2 phase required for efficient displacement at the pore level, though the continual competition between viscous instability and extraction left some residual oil. The fact that the residual saturation was small (and must have contained considerable dissolved CO_2), suggests that the length required to develop miscibility was also small, probably of the order of a few pore lengths. Clearly, in the secondary displacement of crude oil, the CO_2 displaced nearly all of the oil it contacted.

Just after the appearance of a second phase, long, gently curved interfaces were observed. The appearance of the interfaces between the CO_2-rich and oil-rich phases suggested that interfacial tensions were significantly lower than typical oil-water tensions. Because the saturation of the oil-rich phase was always low, however, the two-phase flow allowed by the low interfacial tensions in the relatively large pores of the networks probably did not greatly affect recovery. In regions of the model where two phases were present, deposition of black material, presumably asphaltenes, was also observed. The amount of material precipitated was small, however, and there was no evidence of any restriction to flow caused by the precipitate.

Immiscible Displacements

The performance of the CO_2 and N_2 displacements at low pressure contrasted sharply with that of the high pressure CO_2 flood. In those displacements, the interfacial tensions between the low density CO_2 or N_2 and the oil were much higher than those observed between the CO_2 and the oil at 1200 psia. In both the CO_2 and N_2 displacements, the gas-oil interfaces were tightly curved and moved with a succession of Haines jumps (Haines 1930). The motion of the interfaces was similar to that observed when a refined oil displaced water (see §3.3). In such displacements, injection of N_2 or CO_2 causes all of the interfaces between injected gas and the oil to move slowly into the pore throats blocking their passage to the next pore. Eventually, an interface reaches the narrowest part of the largest available pore throat and jumps into the next pore. The process then continues with each jump occurring in the largest available pore throat. Figs. 3.9 and 3.10 show the distributions of oil and injected gas at breakthrough for the low pressure CO_2 and N_2 displacements. Though there were slight differences, in both displacements the lower part of the model, in which a flow path of slightly larger pores existed, was swept, while large amounts of oil were left elsewhere. Almost no additional oil was recovered in either displacement after breakthrough. Instead, low viscosity CO_2 or N_2 continued to flow through the swept zone. Evidently, the low pressure drop in the injected gas was insufficient to overcome the capillary forces preventing entry of the gas-oil interfaces into other pores.

Fig. 3.7 shows, for comparison, the distributions of CO_2 and oil in the same micromodel at breakthrough and after about one pore volume of injection in the displacement at 1200 psia. In that displacement, the flow was dominated by the viscous instability which caused preferential flow along the center line between injection and production ports. Capillary forces were not sufficient to force flow through the more permeable lower part of the model. Comparison of Fig. 3.7c and d shows clearly that considerable additional oil was recovered after CO_2 breakthrough, in contrast to the behavior of the low pressure floods.

Table 3.3 compares solubility and extraction behavior of CO_2 and N_2 at the various flood conditions. Solubilities of CO_2 and N_2 were estimated from PVT experiments at a slightly higher temperature (90°F) for mixtures of CO_2 and N_2 with Wasson crude oil (Taylor 1984), as previously reported carbon number distributions (see Fig. 3.9 of Orr & Taber 1982) indicate. Extraction of hydrocarbons by CO_2 was estimated from CMC experiments (Orr, Silva & Lien 1983; Silva et al 1981b and c) at 800 and 1200 psia with Maljamar crude oil at 90°F. No direct measurements of extraction by N_2 were made, but comparison of the N_2 and CO_2 densities suggests that extraction of hydrocarbons by N_2 would not be more efficient than by CO_2.

As can be seen from Table 3.3, the sequence of N_2 and CO_2 floods compares the displacement efficiency of fluids with low solubility and little

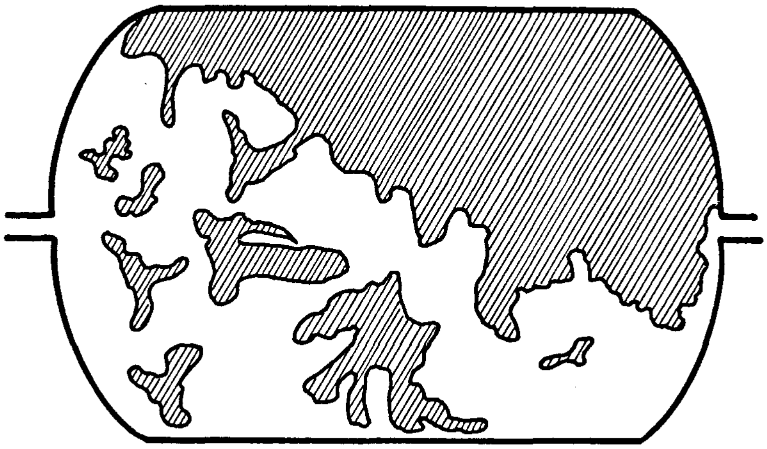

Fig. 3.9 Distribution of oil and gas at CO_2 breakthrough in a secondary displacement of Maljamar crude oil at 25°C and 5.52 MPa.

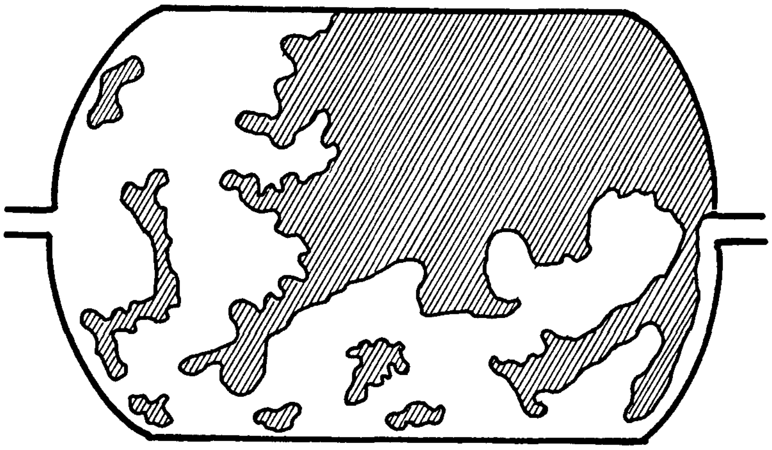

Fig. 3.10 Distribution of oil and gas at N_2 breakthrough in a secondary displacement of Maljamar crude oil at 25°C and 5.52 MPa.

Table 3.3 Solubility and Extraction for Mixtures of N_2 and CO_2 with Maljamar Crude Oil

Fluid	T (°C)	P (psia)	Solubility in Maljamar Crude Oil (mol %)	Extraction of Hydrocarbons from Oil (wt. %)
N_2	25	800	~10	<1
CO_2	25	800	~60	~1
CO_2	25	1200	~70	~20

Table 3.4 Results of Contact Angle Measurements

Fluids	Glass	θ_r	θ_{det}
Dyed Soltrol-Water	HF etched micromodel glass	20.5, 22.5	59, 71, 66.5, 71.5
Dyed Soltrol-Water	UV cell	13, 26, 13, 20 15, 21, 17.5, 16.5, 15.5, 16.5	*
Maljamar Crude Oil-Water	HF etched micromodel glass	**	135.5, 132.5, 132.5, 132
Maljamar Crude Oil-Water	UV cell	25, 16.5, 20, 16.5 17.5, 15.5, 17.5 16, 19.5, 16 23.5, 18	126, 126, 121, 127.5 132.5, 136, 77, 133

*Red-dyed Soltrol did not stick to the smooth glass of the UV cell.

**Immediately after oil contacted the micromodel glass, oil climbed up the outside of the buret, pulling oil away from the surface and increasing the contact angle.

extraction (N_2), high solubility and low extraction (CO_2 at 800 psia), and high solubility and high extraction (CO_2 at 1200 psia). The large difference in solubility between the N_2 and CO_2 at 800 psia did not produce a comparable increase in oil recovery, though the CO_2 did appear to recover slightly more oil than the N_2. The increase in extraction efficiency of the dense, liquid CO_2 phase that formed at 1200 psia, on the other hand, produced a large increase in displacement efficiency, even though the solubility of CO_2 in the oil was only slightly higher at 1200 psia than that at 800 psia. That behavior is consistent with simulations of secondary displacements reported by Orr, Silva and Lien (1983). They found that an increase in solubility does cause some increase in recovery because the fraction of the remaining oil phase that is actually oil is reduced, but that solubility alone cannot explain the very high recoveries observed for some CO_2 floods. Efficient extraction, however, can produce very high local displacement efficiency. Thus, Doscher and El-Arabi's (1981) statement that "...it is the rate of change of solubility with pressure that affects the rate of change of recovery with pressure..." is not supported by the observations reported here.

3.3 Tertiary Displacement Experiments

Three tertiary displacements were also performed in each network:

(6) Displacement of waterflood residual red Soltrol by blue Soltrol at 8.3 MPa (1200 psia).

(7) Displacement of waterflood residual red Soltrol by CO_2 at 8.3 MPa (1200 psia).

(8) Displacement of waterflood residual Maljamar crude oil by CO_2 at 8.3 MPa (1200 psia).

Two additional displacements were performed in micromodel 3:

(9) Displacement of waterflood residual Maljamar crude oil by CO_2 at 5.52 MPa (800 psia).

(10) Displacement of waterflood residual Maljamar crude oil by N_2 at 5.52 MPa (800 psia).

In all the displacements, the model was filled first with water, flooded with oil to an irreducible water saturation and then waterflooded. The waterfloods were conducted at a capillary number of about 2×10^{-6}, low enough that capillary effects dominated the trapping of residual oil. A detailed discussion of trapping in pore networks like those used here has been given by Chatzis, Morrow and Lim (1983).

Displacement (6) examined the behavior of an ideal miscible displacement, one in which the displacing solvent was more viscous than water and first contact miscible with the residual oil. In displacement (7), the CO_2 was still miscible with the oil, but it had a much lower viscosity than either the oil or water. In addition, the CO_2 could dissolve in and diffuse through the water. In displacement (8), effects of phase behavior, viscous instability, and solubility of the CO_2 in the water were all present. Displacements (9) and (10) were performed to examine the effects of the solubility of injected fluid in the oil in tertiary displacements.

First Contact Miscible Displacements

Fig. 3.11 illustrates some of the difficulties which can affect a tertiary displacement. Fig. 3.11a shows the distribution of residual oil for displacement (6) in model 3, and Fig. 3.11b shows the distribution of red oil, solvent (blue oil) and water at solvent breakthrough (0.15 PV). As Fig. 3.11b indicates, much of the injected solvent simply resaturated areas previously occupied by water. Significant portions of the red oil were reconnected with injected solvent, but little oil was driven ahead of the solvent as an oil bank. The first oil production and solvent breakthrough occurred almost simultaneously. Fig. 3.12 is a sketch of actual ganglia which occurred during displacement (6). The red oil in the dendritic ganglia was displaced from its original position, but eventually was driven into pores from which no exit could be traversed at the capillary pressure available to the blob. At that point, the red oil ceased to flow, but continued to diffuse out of the dendritic blob into the flowing stream of blue oil. Finally, significant portions of the residual oil remained trapped, uncontacted by solvent.

Fig. 3.13 shows distributions of red oil, CO_2 and water at CO_2 breakthrough in displacement (7). Because CO_2 was much less viscous than the water or Soltrol, it did a poor job of moving water and hence contacted little of the oil directly. Consequently, breakthrough occurred early at 0.037 PV injected. Thus, the initial performance of the tertiary CO_2 flood was poorer than that of the corresponding tertiary Soltrol flood.

There was, however, one important favorable effect present in the CO_2 flood which did not occur in the Soltrol displacement. CO_2 is sufficiently soluble in water that it can diffuse through the water to reach trapped oil droplets. To study qualitatively the effects of diffusion through the water, flow through the model was stopped, though pressure was maintained, and the model left overnight. After 21 hours, there was clear evidence of redistribution of the oil and water phases, as must happen if CO_2 diffuses into and swells isolated oil droplets. Then, flow through the model was started again, and individual isolated ganglia close to the flowing CO_2 stream were observed. Fig. 3.14 shows the change in size of one ganglion as time passed. Eventually, that ganglion swelled enough to break a water interface separating it from the flowing stream. In addition, after a full day of flow, a second flow channel formed near the top of the model. Thus, though the time scales for such behavior are different in reservoir rocks, it is clear that CO_2 can reach isolated droplets which would be inaccessible to an injected solvent which could not diffuse through water.

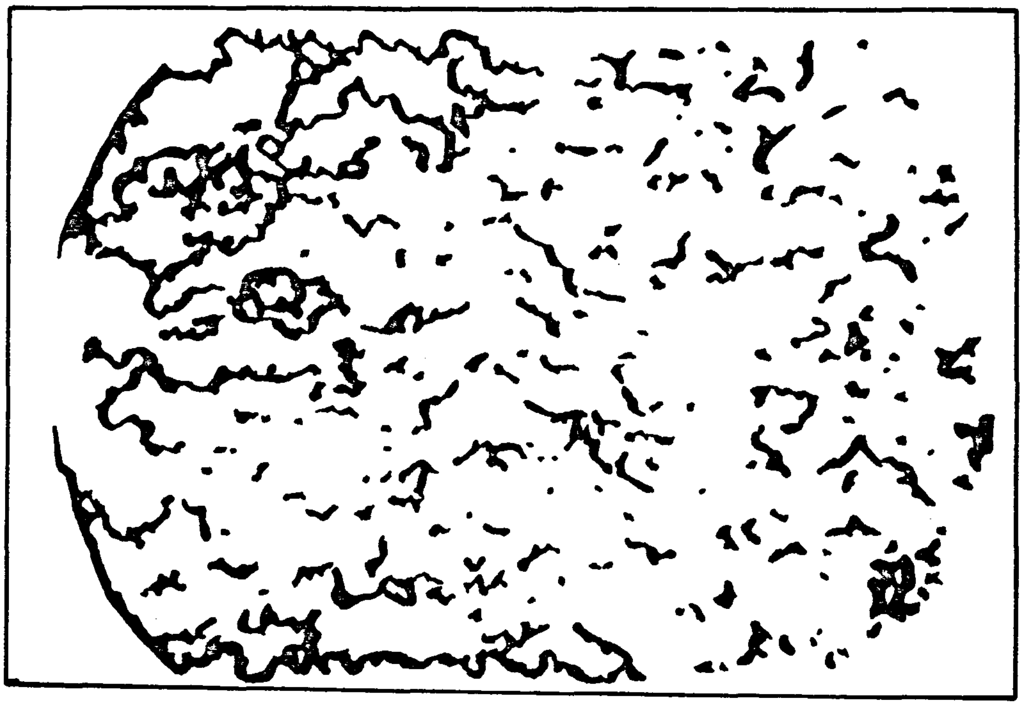

a. RESIDUAL OIL SATURATION

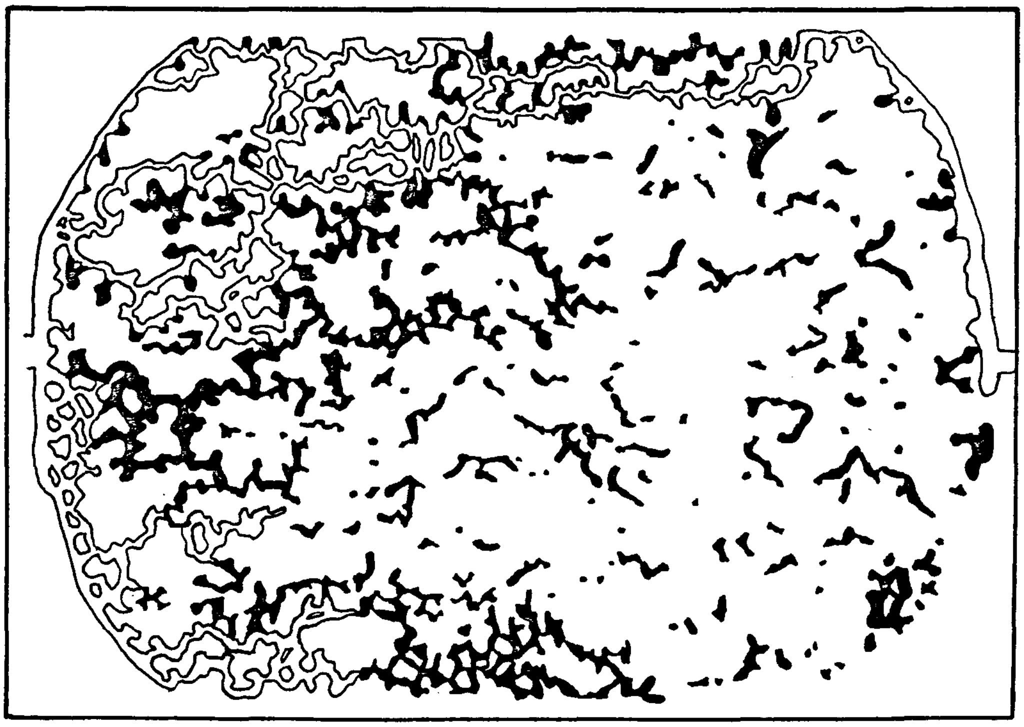

b. SOLVENT BREAKTHROUGH

Fig. 3.11 Tertiary displacement of red Soltrol by blue Soltrol in micromodel 3. The dark areas represent red Soltrol, outlined areas, blue Soltrol and clear areas, water.

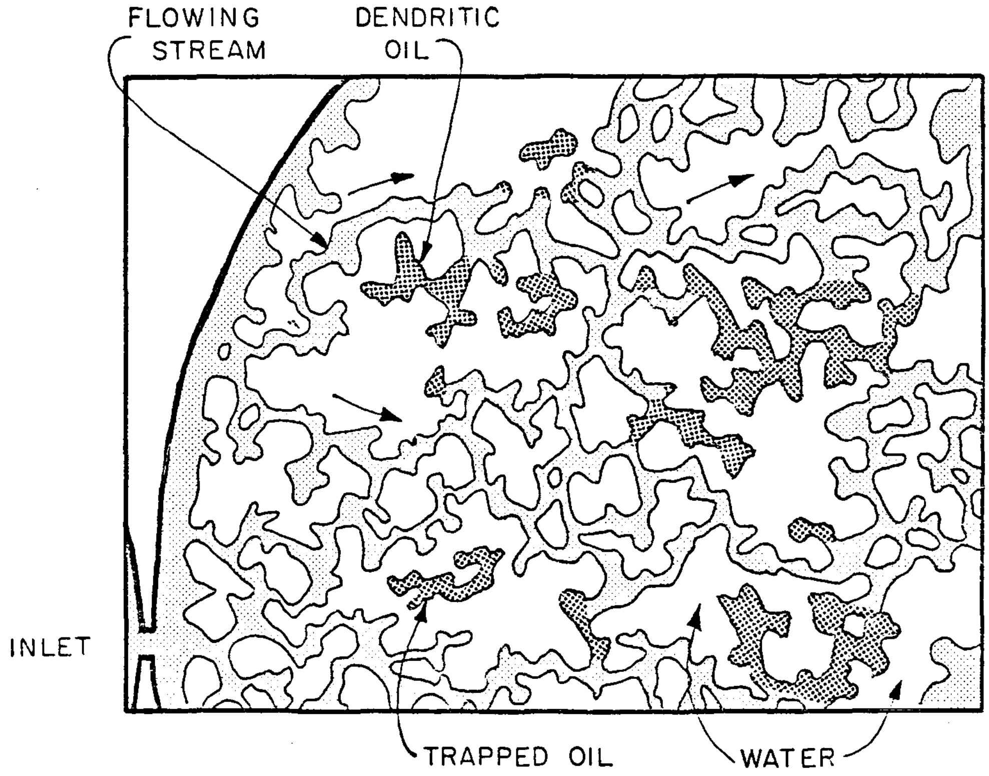
FLOWING STREAM
DENDRITIC OIL
INLET
TRAPPED OIL
WATER

Fig. 3.12 Dendritic and trapped oil saturations during a tertiary displacement of red Soltrol by blue Soltrol in micromodel 3.

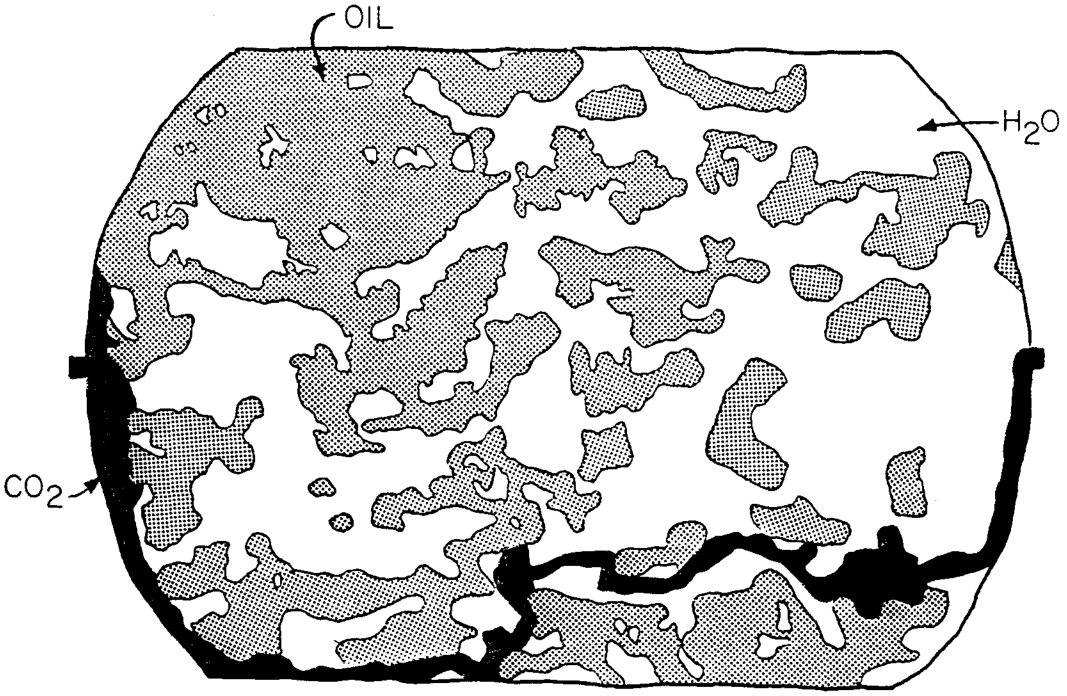

Fig. 3.13 Distribution of oil and water at CO_2 breakthrough in a tertiary displacement of red Soltrol by CO_2 at 25°C and 8.3 MPa in micromodel 3.

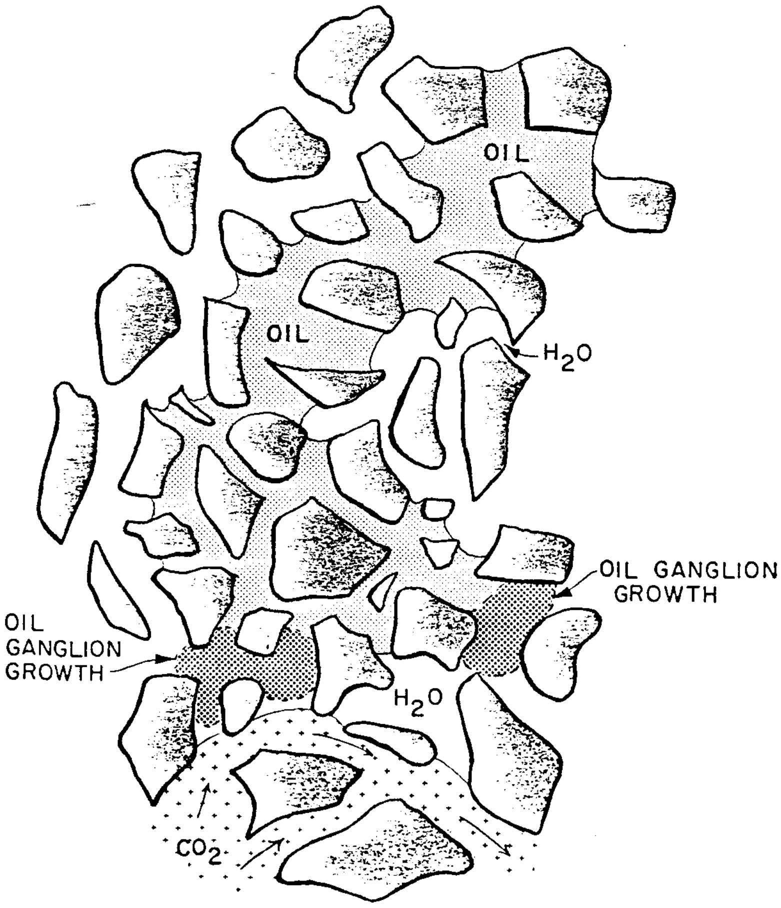
OIL
OIL
H_2O
OIL GANGLION GROWTH
OIL GANGLION GROWTH
H_2O
CO_2

Fig. 3.14 Swelling of isolated oil by CO_2 diffusing through surrounding water.

Multiple Contact Miscible Displacements

The tertiary displacement of Maljamar crude oil contrasted sharply with that of the Soltrol. In the crude oil displacement, many more flow channels developed simultaneously. In addition, two-phase flow was observed throughout the model. Fig. 3.15 was traced from a photograph of pores in which both one and two phase flow of CO_2-oil mixtures was observed. In the pores to the right (downstream) side, a single phase of oil containing enough dissolved CO_2 to lighten its color was observed. In pores on the lower left side, the CO_2 concentration was high enough that the first bubbles of CO_2-rich liquid phase appeared. Then flow of both phases continued for a considerable period. At times, nearly all of the oil was displaced only to be replaced by more oil-rich phase driven from upstream pores. While significantly more two-phase flow occurred in tertiary than in the secondary displacements, and more residual oil was left after the CO_2 flood, the oil recovery was still quite high. Low interfacial tension may have contributed to the high oil recovery. Many droplets of CO_2-rich liquid were observed to pass easily through constrictions which would have stopped typical oil-water interfaces at similar flow rates. Fig. 3.16 shows an example of the passage of a droplet of CO_2-rich phase through such a constriction.

In the displacement of crude oil, the CO_2 contacted the residual oil much more efficiently than it did in the displacement of Soltrol. The most likely explanation for the dramatic difference in behavior lies in differences in the wetting behavior of the Soltrol-water and crude oil-water systems, coupled with the geometry of the pores. Two sets of contact angle measurements were made to examine wetting behavior of dyed Soltrol and Maljamar crude oil on glass. In the first set, contact angles (measured through the water phase) were found to change with time and reached high limiting values for both the Soltrol-water system (135-140°) and the crude oil-water system (140-160°). Subsequent tests indicated, however, that the values obtained may have been an artifact of the experimental technique, so additional measurements were made. The technique used in the second set of measurements is illustrated in Fig. 3.17. Measurements were made on samples of the glass from which the micromodels were made. Those samples were etched briefly with hydrofluoric acid and then cleaned with the same procedure as was used to clean the micromodels between displacements. Measurements were also made for the smooth glass surface of the UV cell used to hold the liquids. A drop of oil was placed in contact with the glass plate. The oil drop was then expanded and the receding contact angle, θ_r, measured. Then, the volume of the oil drop was decreased until the drop detached from the buret. The contact angle of the detached oil drop was then measured.

Results of those measurements are summarized in Table 3.4. Both fluid systems showed considerable contact angle hysteresis as well as scatter typical of most contact angle measurements. Receding contact angles for the Soltrol-water system were around 20° on both the etched micromodel and smooth UV cell glass. Contact angles of 60-70° were observed for the detached Soltrol drops on the etched glass. The Soltrol drops floated off the smooth glass surface, so contact angles were not measured for detached drops on that surface. Receding angles for the crude oil-water system on the smooth UV cell glass were about the same as for the Soltrol-water system. Receding angles

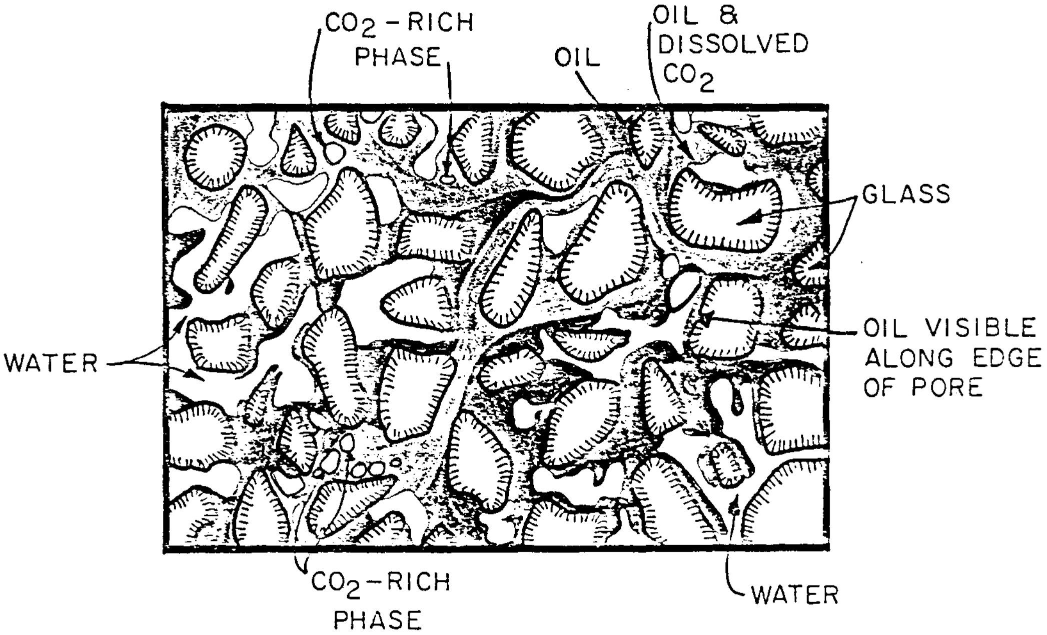
CO2-RICH PHASE
OIL
OIL & DISSOLVED CO2
GLASS
OIL VISIBLE ALONG EDGE OF PORE
WATER
CO2-RICH PHASE
WATER

Fig. 3.15 One- and two-phase flow of CO_2-crude oil mixtures during displacement of Maljamar crude oil by CO_2 at 25°C and 8.3 MPa in micromodel 3.

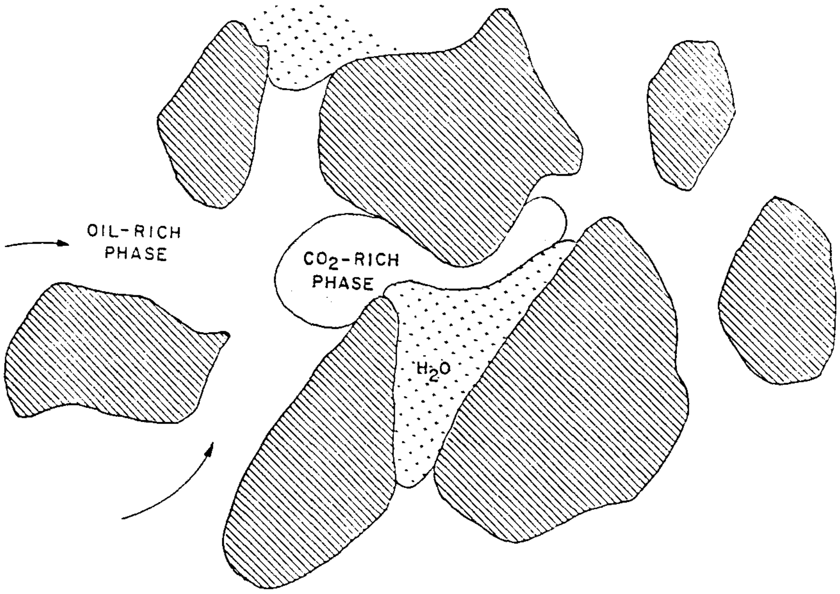
OIL-RICH PHASE
CO2-RICH PHASE
H2O

Fig. 3.16 Flow of droplets of CO_2-rich phase through tight constrictions.

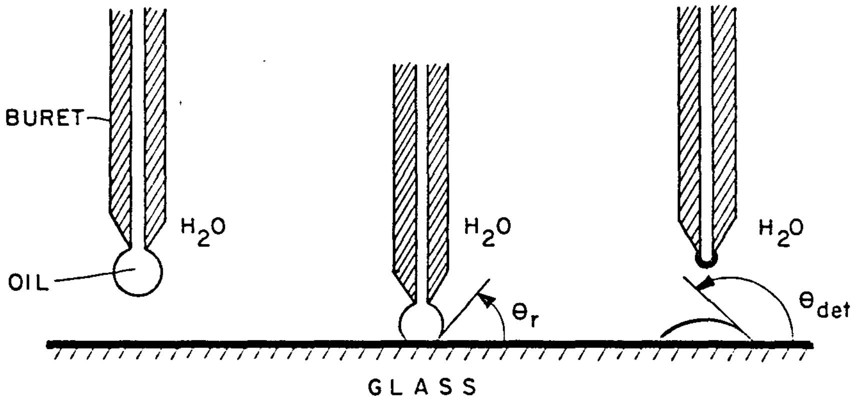
BURET
OIL
H_2O
H_2O
θ_r
H_2O
θ_{det}
GLASS

Fig. 3.17 Procedure for measurement of contact angles.

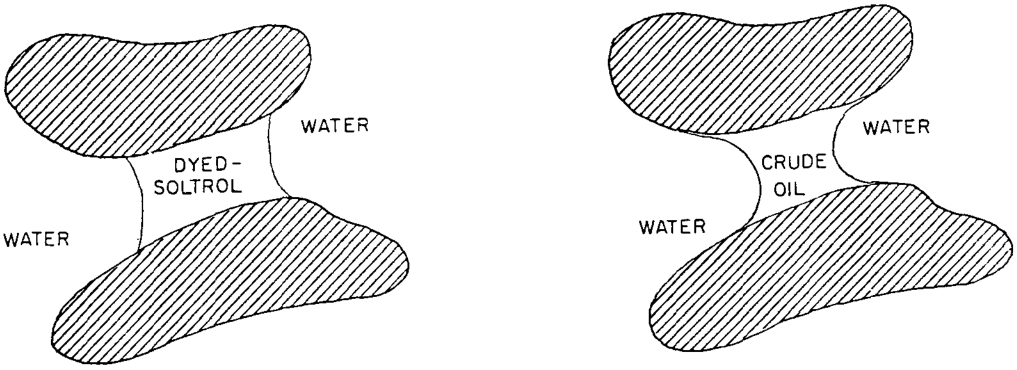
WATER
DYED-SOLTROL
WATER
WATER
CRUDE OIL
WATER

Fig. 3.18 Interface configurations traced from photographs of the same pore in micromodel 3.

were not measured for the etched glass because immediately after the oil contacted the micromodel glass it climbed up the outside of the buret, pulling oil away from the surface and increasing the contact angle. Contact angles for the detached crude oil drops were much higher (125-135°) than for Soltrol drops. Once detached, the crude oil drops spread out to form flattened drops quite different from the round drops formed by the dyed Soltrol. Thus, where crude oil contacted the etched glass during displacements in the micromodels it came closer to wetting the glass surface than did the Soltrol. Observations of oil-water interfaces in the models also indicated that crude oil contact angles were higher in the models, as shown in Fig. 3.18. Water-Soltrol interfaces appeared to exhibit contact angles not greatly different from 90° while water-crude oil interfaces appeared to have contact angles near 180°. In several places in the photograph from which Fig. 3.15 was taken, oil could be seen along the edges of the pores filled with water.

One effect of the differences in contact angles between the Soltrol and the crude oil may have been to alter which fluid, oil or water, occupied the groove at the edge of the pores. Concus and Finn (1969) showed that one fluid will fill completely a groove made from two flat surfaces intersecting at an angle 2β provided that the contact angle θ satisfies

$$\theta < \frac{\pi}{2} - \beta \qquad (3.1)$$

Eq. (3.1) implies that for a given angle β the groove would be filled completely with oil if the contact angle measured through the water satisfied

$$\pi - \theta_{wo} < \frac{\pi}{2} - \beta \qquad (3.2)$$

The grooves at the edges of the pores in the networks used here are not bounded by plane surfaces, though the constraint in eq. (3.2) is still valid (Mason & Morrow 1983). Instead, the pores have lens-shaped sections (Fig. 3.2). If such pores are modeled as bounded by intersecting circular arcs, as shown in Fig. 3.19, then the shape of the pore can be characterized by a single parameter F. As F goes to zero, the pore becomes a slot. If F is one, the pore has a circular cross section. It can be shown (Campbell 1983a) that the half angle between the surfaces is given by

$$\beta = \sin^{-1}\ [2F/(1 + F^2)] \qquad (3.3)$$

Thus, as F decreases from one, the groove will be filled with oil for smaller values of θ_{wo}, or larger contact angles measured through the oil phase. Fig. 3.20 shows the calculated relationship between F and the critical contact angle. For contact angles greater than 90°, oil can fill the capillary groove if the pore is large enough (F is small enough). If the contact angle is less than 90°, oil cannot fill the groove exclusively.

In the networks used here, a range of values of F existed. For instance, for model 3, the smallest pore throats probably had values of F near 0.4-0.6 (Table 3.1) while the largest pores had values near 0.1. As Fig. 3.20 indicates for the contact angles given in Table 3.4 for detached drops, the

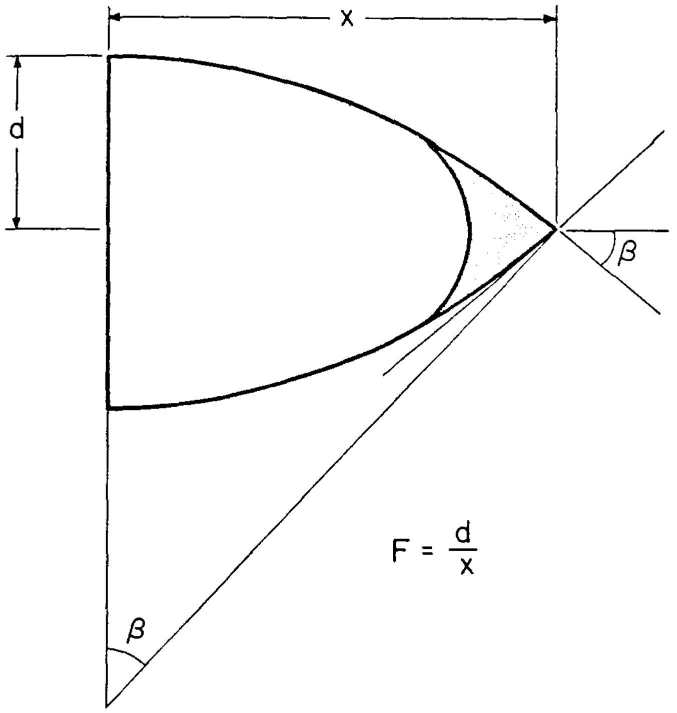

Fig. 3.19 Lens-shaped idealization of a pore cross section.

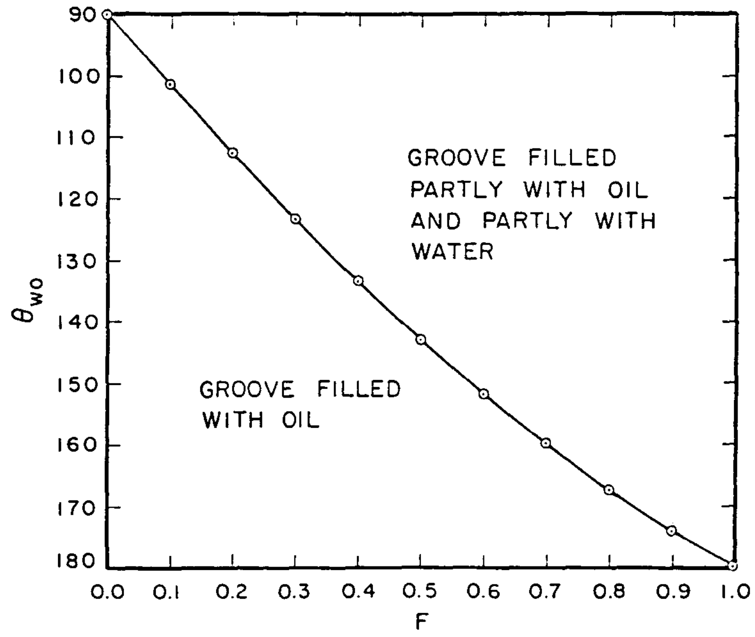

Fig. 3.20 Contact angles required for oil to fill grooves bounding pores of various sizes.

grooves in the largest pores were probably occupied by crude oil but not by Soltrol. Since the model was saturated first with water and then flooded with oil to irreducible water saturation, there was almost certainly plenty of opportunity for the crude oil to contact and spread on the glass surfaces. In the small pores contact angles in the neighborhood of 135-150° were required for oil to be present in the grooves in the pore throats. Thus, there may have been some small pores in which the oil films were not continuous. CO_2 entering such a pore would be forced to overcome capillary pressure differences and displace water.

Thus, observations of interfaces and oil films in the models as well as contact angle data suggest that in the displacements of crude oils, continuous, connected paths in the oil phase were more likely to exist. Direct observations indicated clearly that in some pores which contained both oil and water, the CO_2-rich phase flowed in the oil-filled portion of the pore. Hence, it appears that the presence of more connected oil paths could account for the fact that CO_2 contacted more oil in the displacements of crude oil.

Immiscible Displacements

Figs. 3.21 and 3.22 show distributions of oil, water and injected fluid for the tertiary CO_2 and N_2 displacements at 800 psia. In those displacements, the low density vapor phases were clearly the most nonwetting of the phases present. In both floods, a single flow channel was swept by the injected vapor. The path swept was similar to that of the tertiary CO_2-red oil displacement described previously. Strongly curved interfaces were observed between injected vapor and both oil and water. The interfaces penetrated slowly into pore throats and then jumped rapidly into adjacent pore bodies (Haines 1930). Water was displaced inefficiently in both cases as might be expected for immiscible displacements with such adverse mobility ratios. Even when oil blobs were encountered, the CO_2 and N_2 displaced little of the oil. On the time scale of the experiments, the much higher solubility of the CO_2 in the oil appeared to produce little additional oil recovery, probably because so little of the residual was contacted. Presumably, if enough time were allowed for CO_2 to diffuse through the water to reach the trapped oil, swelling might cause some additional oil to be recovered. The amount recovered might still be small, however, since even when oil was contacted by the injected fluid, it was not necessarily displaced by the immiscible vapor. At least some of the swelling would simply cause resaturation of areas occupied by water with swollen oil.

The results of the immiscible displacements provide additional evidence that extraction also played a very important role in the high pressure tertiary floods. Extraction of hydrocarbons from the oil generated mixtures which could flow through the connected films of oil in the capillary grooves at the edges of the pores. Though interfaces between oil-rich and CO_2-rich phases were observed, the interfacial tensions were apparently low enough that the CO_2-rich phase was not driven to flow only through the largest pore throats, as was the case in the low pressure displacements.

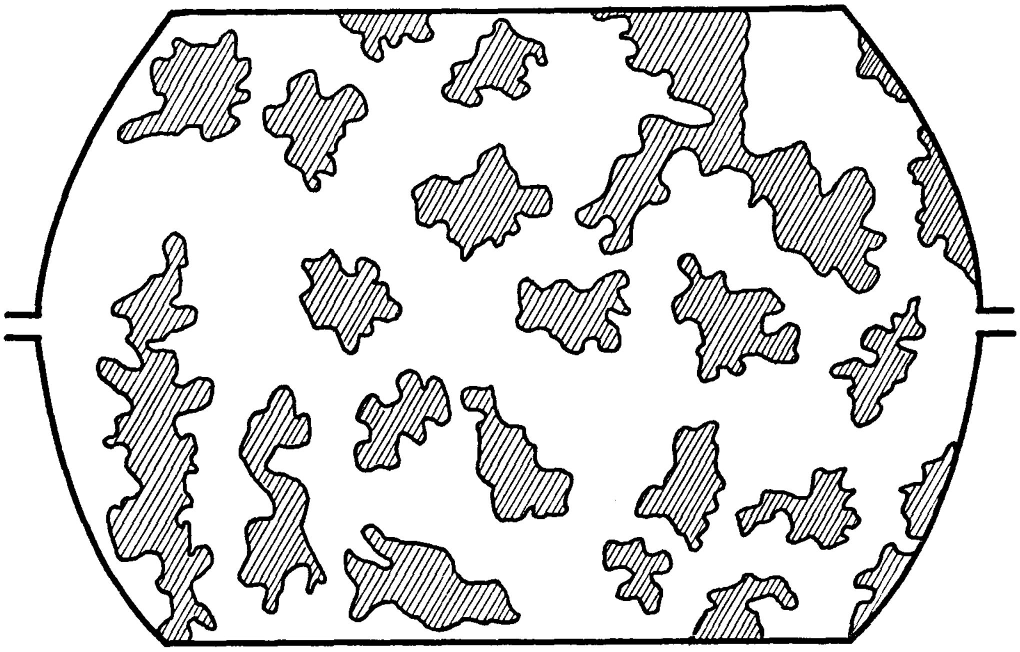

a. Residual oil saturation

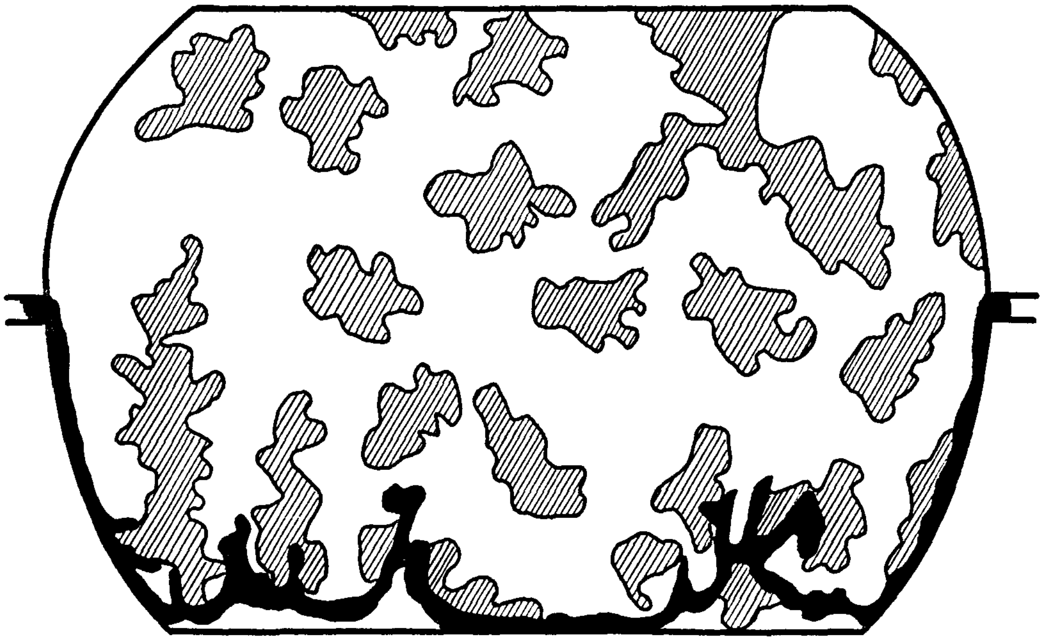

b. CO_2 breakthrough

Fig. 3.21 Tertiary displacement of Maljamar crude oil by CO_2 at 25°C and 5.5 MPa. Shaded areas represent oil, dark areas, CO_2 and clear areas, water.

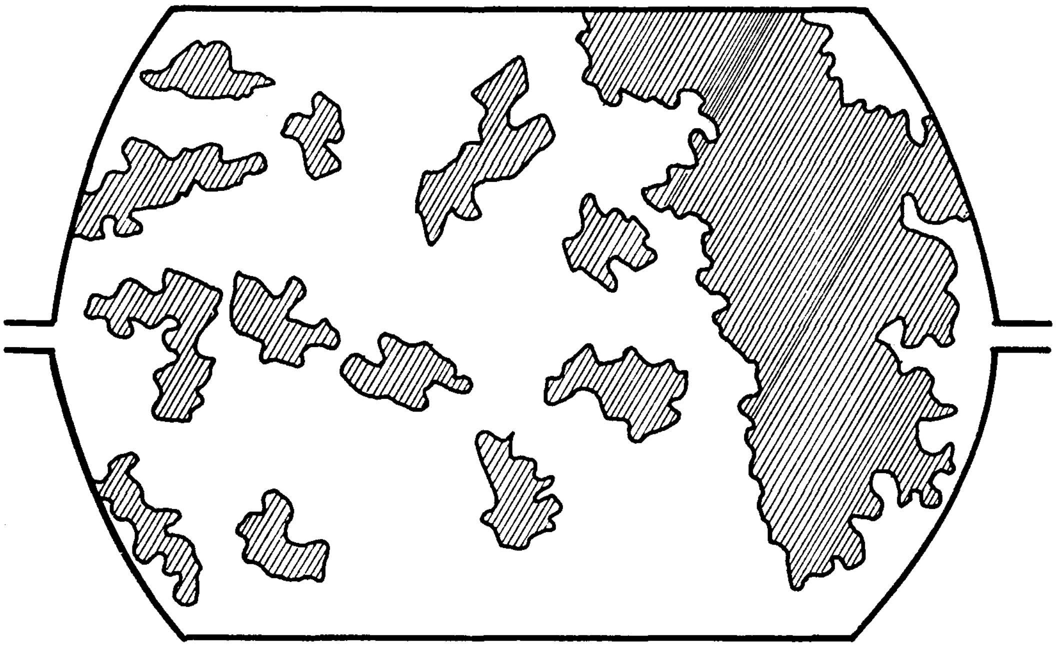

a. Residual oil saturation

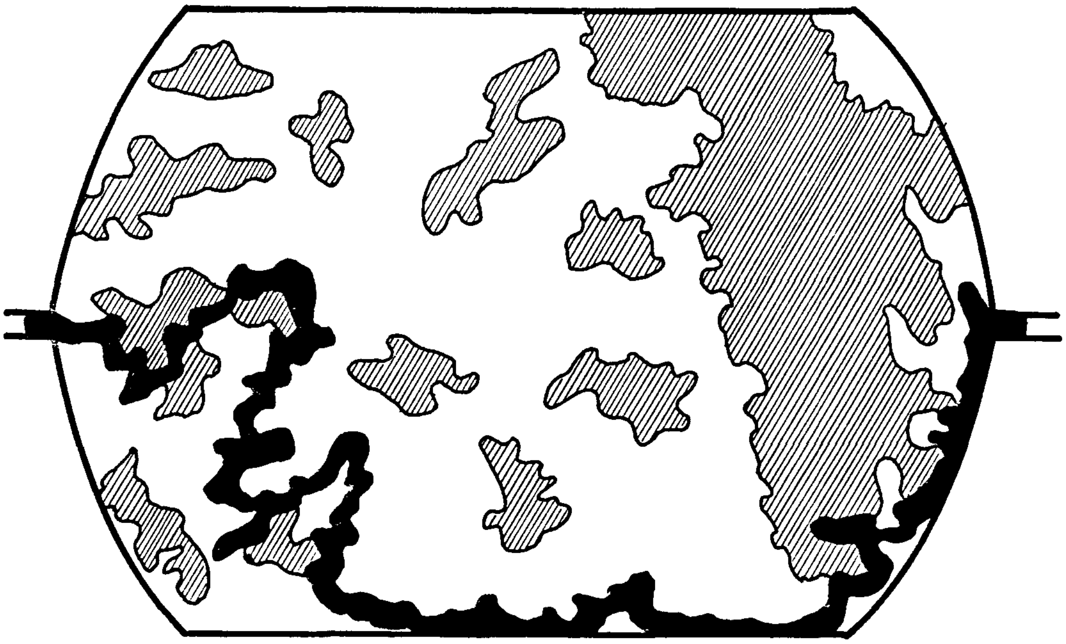

b. N_2 breakthrough

Fig. 3.22 Tertiary displacement of Maljamar crude oil by N_2 at 25°C and 5.5 MPa. Shaded areas represent oil, dark areas, CO_2 and clear areas, water.

Doscher, Oyekan and El-Arabi (1983) also considered mechanisms of oil recovery in tertiary CO_2 and N_2 floods. They performed gravity stabilized displacements in partly scaled models packed with sand and found that N_2 and CO_2 recovered about 55 and 75% of the residual oil to a waterflood. They argued that the recovery was due to a reduction of the residual oil saturation due to gas injection. The gravity stabilization allowed most of the mobile water to be displaced, so that the residual oil saturation could be reached by the injected fluid. In the experiments reported here, gravity effects were absent from the displacements since the models were horizontal. It appears, therefore, that while a reduction of the residual oil saturation may augment recovery in some gravity stabilized displacements, it is not the only mechanism which leads to oil recovery when dense CO_2 is injected.

3.4 Recovery of Oil from Dead-End Pores

It is clear from the tertiary experiments described above that oil can exist in droplets given the shape of dead-end pores by surrounding water, whether or not the porous medium contains any true dead-end pores. To study qualitatively the mixing of CO_2 and oil in dendritic oil ganglia, a series of displacements was conducted in a micromodel (Fig. 3.1) which contained several true dead-end pores. Five displacements were performed:

(11) Red Soltrol recovered from the dead-end pores by blue Soltrol.

(12) Red Soltrol recovered by CO_2.

(13) Maljamar crude oil recovered by CO_2.

(14) Red Soltrol shielded by water recovered by CO_2.

(15) Maljamar crude oil shielded by water recovered by CO_2.

All of the CO_2 displacements were conducted at 25°C and 8.3 MPa (1200 psia). Displacements (11) and (12) were performed to compare the recovery of oil by a solvent which is first contact miscible with the oil. Effects of phase behavior were present in displacement (13). Displacements (14) and (15) were designed to confirm that CO_2 could diffuse through water to reach trapped oil. In all the experiments, the injection rate was 2.0 cm^3/hr which yielded a flow velocity of about 1.2 mm/sec in the central channel.

Because the dead-end pores were quite large, the recovery of oil by diffusion alone was slow. Red Soltrol was completely replaced by blue Soltrol (displacement 11) after about 64 hours. In contrast, the red Soltrol (displacement 12) was recovered after about 3.5 hours when CO_2 was the flowing fluid. Clearly, diffusion proceeded more rapidly in CO_2 than it did in the Soltrol.

The recovery of Maljamar crude oil by CO_2 (displacement 13) was far more rapid than would be expected if diffusion alone were responsible. Shortly after CO_2 injection began, an interface between the CO_2 and the oil formed at the inlet of each pore. The interface traversed the pore neck in about 130 seconds until it reached the body of the pore (Fig. 3.23a). As the interface moved, oil-rich liquid was drawn through the groove at the edge of the pore neck (Fig. 3.23b). Dark oil could also be seen being driven along the grooves at the edge of the central flow channel. As it was displaced downstream, more oil-rich liquid was drawn from the groove in the pore neck to replace the liquid in the flow channel. Occasionally, oil-rich liquid bridged the pore neck, slowing movement of the interface temporarily. Bridging also occurred just upstream of the pore neck in the flow channel. The resulting lamella was then displaced downstream.

Precipitation of asphaltic material was observed in the pore neck and pore body. Apparently, precipitation was associated with the interfaces between the CO_2-rich liquid and the oil-rich liquid. Darker lines of precipitate were observed at positions where the interface paused.

Removal of all of the oil-rich liquid occurred in about 5 minutes. Evidently, the recovery of oil from the dead-end pore was dominated by capillary forces. The oil-rich phase preferentially wet the glass and hence occupied the grooves at the edges of the pores. As that liquid was driven downstream in the flow channel, capillary forces acted to draw more oil out of the pore to replace that oil displaced. The mechanism described here is partly the result of the fact that nearly pure CO_2 forms a second phase when mixed with crude oil and partly the result of the special geometry of the dead-end pores and their edge grooves. Whether a mechanism of this sort operates in reservoir rocks is not known.

Fig. 3.24 illustrates results typical of the displacements (14 and 15) in which CO_2 flowed past dead-end pores that contained red Soltrol or crude oil with water filling the pore neck. To fill the dead-end pores, the model was partially evacuated, and oil was allowed to flow into the pores. When the pressure had equalized, a small vapor bubble remained in each pore. Then water was injected, and the pressure was raised to 8.3 MPa (1200 psia). At that pressure, the vapor bubble collapsed, and water filled the pore neck. Then CO_2 flow was started, and the motion of the water interface observed.

Results for the refined oil and crude oil were similar to those illustrated in Fig. 3.24. As CO_2 diffused through the water, the oil swelled, displacing the water barrier. Eventually, the water film was dislodged by the flowing CO_2, and then the oil in the pore was recovered just as when no water was present. As shown in Fig. 3.24, the water barrier was displaced the length of the pore neck (2 mm) in about 9 hours in the Soltrol case. In the experiment with crude oil, however, the displacement of the barrier through the length of the neck required 51 hours. Because the volumes of water initially present were significantly different, the concentrations of CO_2 in the pore at the time the oil-water interface reached the pore neck must also have been different. Thus, no quantitative information about diffusion coefficients was obtained.

The movements of the water barriers in the experiments described here

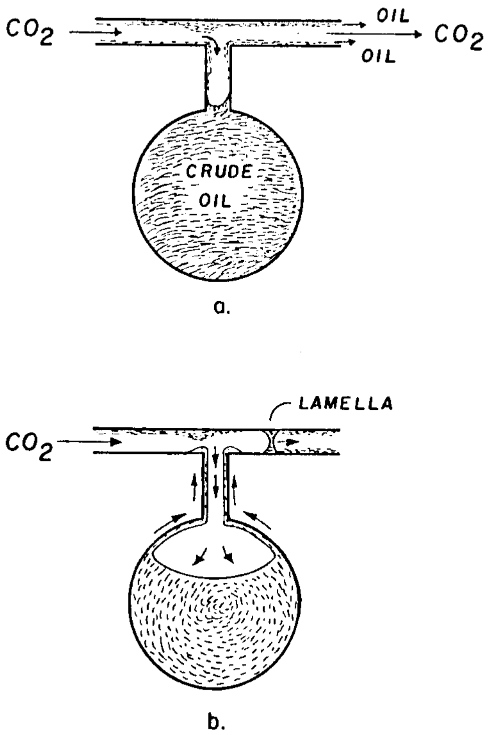

CO_2
OIL
CO_2
OIL
CRUDE OIL
a.
LAMELLA
CO_2
b.

Fig. 3.23 Recovery of Maljamar crude oil from a dead-end pore by CO_2 at 25°C and 8.3 MPa.

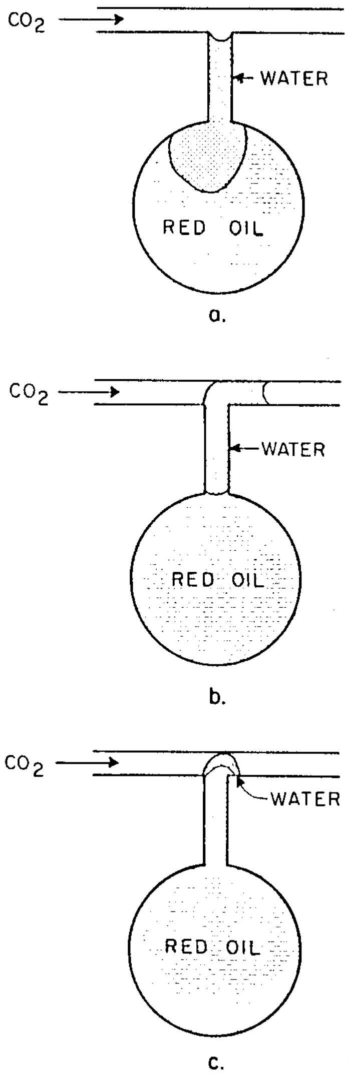

CO_2
WATER
RED OIL
a.
CO_2
WATER
RED OIL
b.
CO_2
WATER
RED OIL
c.

Fig. 3.24 Recovery of red Soltrol isolated by water in a dead-end pore by CO_2 at 8.3 MPa and 25°C. From top to bottom: a. at start of CO_2 injection; b. position of water barrier after 18 hours; c. position of water barrier after 26.5 hours.

provide clear evidence that CO_2 can reach oil isolated by water. Thus, diffusion of CO_2 and consequent swelling of trapped oil droplets may contribute to initial mobilization of residual oil. Because diffusion of hydrocarbons through the water to the flowing CO_2 will be much slower, however, the standard description of the effects of phase behavior which is based on the assumption of complete local mixing, does not apply. The change in the time scales of diffusion and flow alters the local composition path in a way which must alter local displacement efficiency. What is not yet known, however, is the relative importance of such effects for displacements at reservoir scale.

The observations of interface motion suggest that high pressure diffusion coefficients for CO_2 in water and oil could be measured if the pore geometry were simpler. Consider, for instance, the diffusion of CO_2 and a pure hydrocarbon, say decane (C_{10}), in an infinite capillary of uniform cross section (Fig. 3.25). If at time $t = 0$ a barrier between pure CO_2 and pure C_{10} at $x = 0$ is removed, CO_2 will dissolve in the C_{10} and vice versa, and diffusion will begin. If the density and diffusion coefficient of each component can be taken as constant within a phase, then (Danckwerts 1950; Ruschak & Miller 1972)

$$\frac{\partial c_{1c}}{\partial t} = D_{1c} \frac{\partial^2 c_{1c}}{\partial x^2}$$

and (3.4)

$$\frac{\partial c_{1d}}{\partial t} = D_{1d} \frac{\partial^2 c_{1d}}{\partial x^2}$$

where c_{1c} and c_{1d} are the volume fractions of CO_2 in the CO_2-rich and decane-rich phases, D_{1c} and D_{1d} are diffusion coefficients in the two phases, and x and t are length and time. The initial conditions are

$$\begin{aligned} c_{1d} &= 0 \qquad x > 0 \;,\; t = 0 \\ c_{1c} &= 1 \qquad x < 0 \;,\; t = 0 \end{aligned} \tag{3.5}$$

and the boundary conditions far away from the interface are

$$\begin{aligned} \lim_{x \to \infty} c_{1d} &= 0 \qquad t > 0 \\ \lim_{x \to -\infty} c_{1c} &= 1 \qquad t > 0 \end{aligned} \tag{3.6}$$

At the interface between the phases, each component must satisfy a material balance based on the idea that there is no accumulation of material at the interface

$$D_{1c} \frac{\partial c_{1c}}{\partial x} - \frac{\rho_{1d}}{\rho_{1c}} D_{10} \frac{\partial c_{1d}}{\partial x} = \left[c_{1c} - \frac{\rho_{1d}}{\rho_{1c}} c_{1d} \right] \frac{d\varepsilon}{dt} \qquad x = \varepsilon,\; t > 0 \tag{3.7}$$

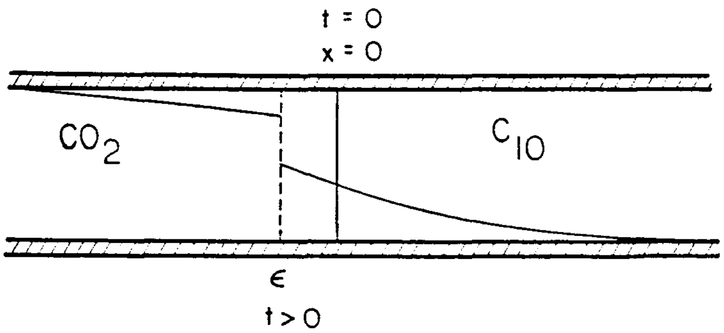
t = 0
x = 0
CO_2
C_{10}
ϵ
t > 0

Fig. 3.25 Movement of a CO_2-C_{10} interface as CO_2 diffuses into the C_{10}.

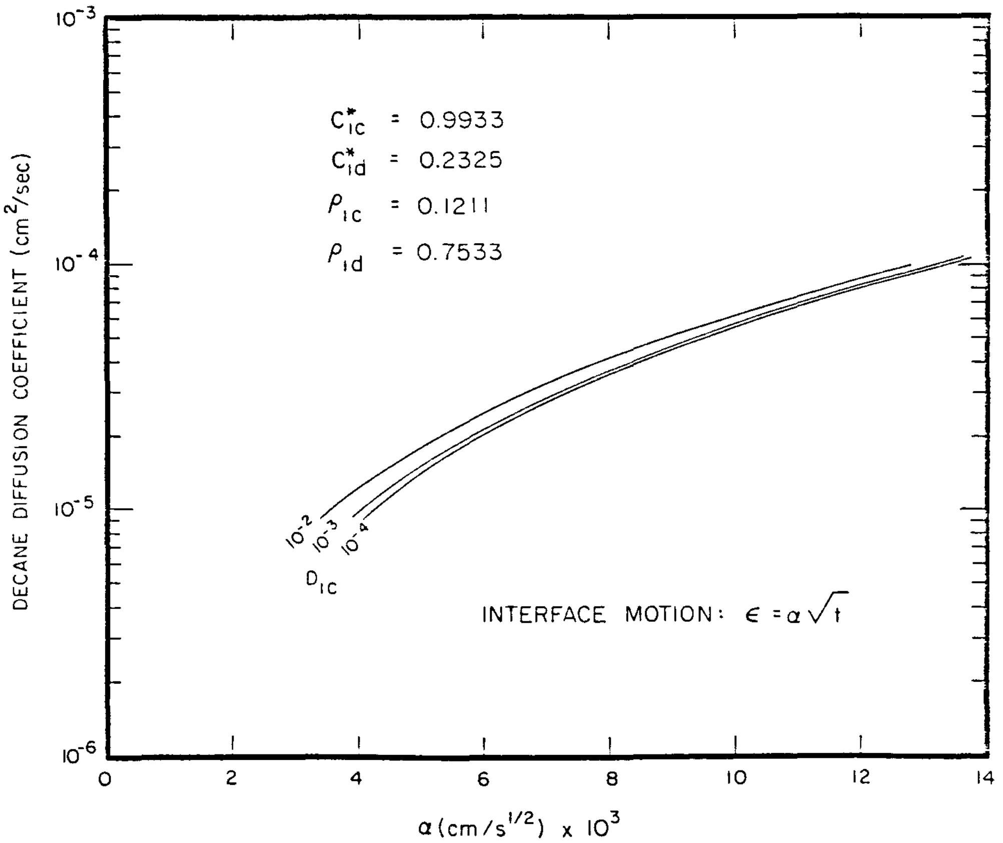

Fig. 3.26 Sensitivity of the rate of interface movement to values of the diffusion coefficients of CO_2 and C_{10} calculated using CO_2-decane phase behavior at 100°F and 700 psia.

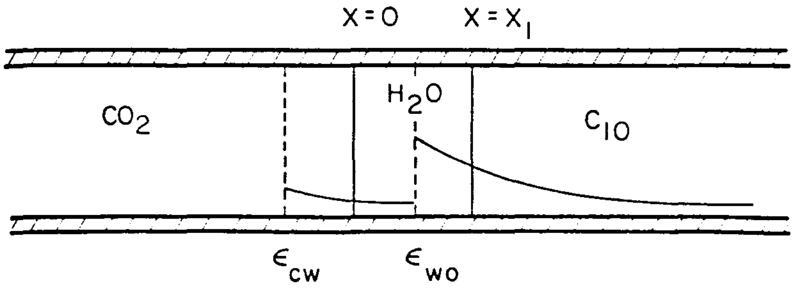
X = 0
X = X_1
CO_2
H_2O
C_{10}
ϵ_{cw}
ϵ_{wo}

Fig. 3.27 Movement of CO_2-water and water-C_{10} interfaces as CO_2 diffuses through the water into the oil.

where ρ_{1d} and ρ_{1c} are the apparent mass densities of CO_2 in the decane-rich phase and CO_2-rich phases, and ε is the position of the interface. Finally, we assume that the phases have their equilibrium compositions c^*_{1c} and c^*_{1d} at the interface

$$\begin{aligned} c_{1c} &= c^*_{1c} \qquad x = \varepsilon^- \ , \quad t > 0 \\ c_{1d} &= c^*_{1d} \qquad x = \varepsilon^+ \ , \quad t > 0 \end{aligned} \tag{3.8}$$

The solution to the differential equations has the form

$$\begin{aligned} c_{1c} &= a + b \operatorname{erf}\left(\frac{x}{2\sqrt{D_{1c}t}}\right) \qquad x < \varepsilon \ , \quad t > 0 \\ c_{1d} &= d + e \operatorname{erf}\left(\frac{x}{2\sqrt{D_{1d}t}}\right) \qquad x > \varepsilon \ , \quad t > 0 \end{aligned} \tag{3.9}$$

The jump condition at the interface, eq. (3.7), can only be satisfied for all t if

$$\varepsilon = \alpha\sqrt{t} \tag{3.10}$$

where α is a constant. The five constants a, b, d, e and α can be determined as the solution to eqs. (3.6), (3.7) and (3.8). Because those equations are nonlinear, a Newton-Raphson iteration was used. Typical results are shown in Fig. 3.26 for CO_2-C_{10} mixtures at 1000 psia and 100°F. Composition and density data used were from Reamer and Sage (1963). In this example, the rate of movement at the interface is relatively insensitive to the diffusion coefficient in the CO_2-rich phase because the solubility of C_{10} in the CO_2-rich phase is low enough that the concentration gradient in that phase remains low. The motion of the interface is dominated by diffusion in the C_{10}-rich phase. Thus, the diffusion coefficient of CO_2 in C_{10} can be determined experimentally from a plot of interface position against $\sqrt{t}$.

Given the diffusion coefficient of CO_2 in the oil phase, the diffusion coefficient of CO_2 in water can be obtained in a similar experiment, as is illustrated in Fig. 3.27. In this version of the experiment, the CO_2 is separated from the C_{10} by a water barrier. As CO_2 diffuses through the water and swells the oil, the CO_2-water and water-oil interfaces move as a result. Because the water barrier has finite length, this problem must be solved numerically, but the approach is the same. The rate of movement of the interface is calculated from the component solubilities and the diffusion coefficient of CO_2 in the oil, with the diffusion coefficient in the water as a parameter. Thus, measurement of the motion of the interfaces provides enough information to obtain the CO_2 diffusion coefficient in the water phase.

3.5 Summary and Conclusions

The experiments described here illustrate mechanisms which must also act, at least in some circumstances, in reservoir rocks, but they were not scaled experiments. Pores in reservoir rocks are smaller, have much wider variations in shape and size, and are connected in three dimensions rather than two. In addition, flow velocities in typical field displacements are an order of magnitude lower. Thus, the ratio of the characteristic time to diffuse a pore diameter to that required to flow a pore length, the microscopic Peclet number,

$$Pe = \frac{ud_p}{D} \tag{3.11}$$

was larger in the pore network displacements than in field displacements. Clearly, the displacements described here do not preserve either the geometry or the time scales of displacements in reservoir rocks, where diffusion to and from dendritic oil and into trapped oil should be more effective. Nevertheless, the physical processes, flow, diffusion, phase behavior, and capillary phenomena, that operate to determine microscopic displacement efficiency in a reservoir rock also operate in the pore network displacements. Thus, displacements of the sort described provide a useful framework for additional work to determine the quantitative relationships between the various mechanisms.

Observations of displacements in two-dimensional pore networks led to the following conclusions:

(1) The length required to develop miscibility in secondary CO_2 floods at high pressure (1200 psia) was significantly less than the length of the pore models.

(2) In those floods a residual oil saturation to CO_2 developed in the region first penetrated by viscous fingers, as predicted by Gardner and Ypma (1982).

(3) Configurations and movements of interfaces between CO_2-rich and oil-rich phases in CO_2-crude oil displacements suggested that the interfacial tensions were significantly lower than typical oil-water tensions. In the high pressure secondary displacements in the models used here, low tensions appeared to have little effect on recovery efficiency because the second phase saturation was always very low. In tertiary displacements at pressures above the MMP, much of the displacement of oil occurred with two phases flowing simultaneously. Hence, low interfacial tension probably had a greater effect in the tertiary displacements.

(4) Secondary displacements of Maljamar crude oil at low pressure (800 psia) by CO_2 and N_2 were relatively inefficient. The amount of residual oil left in both displacements was considerable and

comparable. The higher solubility of CO_2 (60%) than N_2 (10%) increased recovery only slightly.

(5) Multicontact miscible displacement of Maljamar crude oil at high pressure (MMP) contrasted sharply with displacement by CO_2 at low pressure. The results suggest that extraction of hydrocarbon by a dense CO_2 phase accounts for high displacement efficiency.

(6) Displacement of waterflood residual Soltrol by a viscous miscible solvent (Soltrol) was also relatively inefficient. Oil production and solvent breakthrough occurred almost simultaneously. While considerable residual oil was reconnected, much of it was recovered slowly by diffusion from dendritic ganglia given their shape by surrounding water. Significant portions of the residual oil remained uncontacted by the solvent.

(7) Tertiary displacements of residual Soltrol by high pressure CO_2 were also inefficient because the CO_2 did not displace water effectively. Given enough time, however, CO_2 did diffuse through the water to reach and swell trapped oil droplets. Experiments in dead-end pores blocked by water also demonstrated that CO_2 can reach trapped oil where a solvent insoluble in water would not.

(8) High pressure CO_2 contacted residual crude oil much more efficiently that it did residual Soltrol. Observations of oil-water interfaces and independent contact angle measurements indicated that the crude oil wet the glass more strongly than did the Soltrol. Calculations of the conditions under which oil would occupy grooves at the edges of the pores indicated that continuous paths in the oil phase were more likely in the displacements of crude oil. Hence, differences in wetting behavior probably account for the better performance of the tertiary CO_2-crude oil displacements.

(9) Tertiary displacements of residual crude oil by CO_2 and N_2 at low pressure (800 psia) were much less efficient. Significant portions of residual oil remained isolated and uncontacted by solvent. Initial flow patterns were similar to those observed in the first contact miscible displacement of Soltrol by CO_2 (1200 psia). In the Soltrol displacement, any oil contacted by the CO_2 was eventually recovered. In the low pressure CO_2 and N_2 displacements of crude oil, however, reconnection of oil by the injected fluid did not guarantee recovery.

(10) Soltrol diffused more rapidly from dead-end pores into flowing CO_2 than it did into Soltrol dyed a different color. Phase behavior of CO_2-crude oil mixtures gave rise to capillary forces which acted to remove oil from dead-end pores bounded by capillary grooves.

(11) Observations of swelling of oil isolated by water by CO_2 diffusing through the water along with analysis of diffusion in two-phase systems suggest that diffusion coefficients for CO_2 at high pressure can be measured by observation of the motion of CO_2-oil and oil-water interfaces in a capillary tube.

4. MIXING IN RESERVOIR ROCKS

If the phase behavior of CO_2-crude oil mixtures influences local displacement efficiency, then the mixing of injected and in-place fluids that occurs when CO_2, oil and water flow in reservoir rocks must also affect performance. Mixing behavior partly determines the overall compositions of fluid mixtures which form during the displacement, and hence is coupled to the effects of phase behavior. In this chapter we report results of experiments to examine mixing in reservoir core samples when one and two phases are present. Literature pertinent to the investigation is reviewed in §4.1. Experimental equipment and procedures are described in §4.2. In §4.3 results of displacement experiments and their interpretation are discussed, and in §4.4 observations concerning the pore structures of the reservoir core samples examined in thin sections are compared with displacement behavior.

4.1 Literature Review

Single-Phase Displacements

Interpretation of displacement experiments from the compositions of produced fluids presents a challenge even for single-phase displacements in linear cores. In miscible displacements, a transition zone develops between the displaced and displacing fluid. As a displacement progresses, the transition zone grows due to molecular diffusion, to mixing caused by nonuniform flow velocities within individual pores (Taylor 1953) and to the mixing which results from differences in flow path length caused by local small-scale heterogeneity in the porous medium. Measurements of the length of that transition zone, say the distance between the 10 and 90 percent concentrations, can be used to calculate a dispersion coefficient (Perkins & Johnston 1963) based on an analogy between molecular diffusion and dispersion (Aronofsky & Heller 1957), which lumps several mixing mechanisms. Thus, the assumption inherent in many interpretations of experimental work on miscible flooding is that flow in a porous rock can be described by convection-diffusion equations of the form

$$\phi \frac{\partial c}{\partial t} + \nabla \cdot (\underset{\sim}{v} c) - \phi \nabla \cdot D \nabla c = 0 \qquad (4.1)$$

where ϕ is the porosity, $\underset{\sim}{v}$ the Darcy flow velocity, c the local concentration of one component in a binary displacement, and D the dispersion coefficient. Core floods are normally assumed to be one-dimensional, and the velocity is taken as uniform so that

$$\frac{\partial c}{\partial \tau} + \frac{\partial c}{\partial \xi} - \frac{1}{Pe} \frac{\partial^2 c}{\partial \xi^2} = 0 , \qquad 0 \leq \xi \leq 1 \qquad (4.2)$$

where v is the Darcy velocity for flow in the x direction, $\xi = x/L$, $\tau = vt/\phi L$ and $1/Pe = \phi D/vL$, the Peclet number. Thus, in this case, the flow system is characterized by a single parameter, the Peclet number.

The limitations of the simple representation given in eq. (4.2) have been reviewed in some detail by Heller (1963). A fundamental assumption inherent in eq. (4.2) is that the flow is uniform. Heller demonstrated experimentally and theoretically that the assumption of uniform flow is often not satisfied. He performed a miscible flood in which dyed styrene monomer displaced clear styrene in a Berea sandstone core. After about half a pore volume had been injected, the styrene was polymerized and the core sectioned. There was clear evidence of channeling in a sandstone which is usually assumed to be relatively uniform. Heller pointed out that the presence of local nonuniformities does not preclude the use of a model of the form given in eq. (4.2) as long as the scale over which nonuniformities correlate is small compared to the scale of the displacement. An apparent dispersion coefficient determined for such a porous medium would be larger, however, than that for a truly uniform porous medium. Hence, the apparent longitudinal dispersion coefficient appropriate to a field scale displacement could easily be very different from that measured for laboratory cores.

Nonuniform flow fields can arise from nonuniform fluid properties as well as from nonuniform rock properties. Heller's (1963) derivation of the conditions required for uniform flow illustrates the problem nicely. In vector form, Darcy's law is

$$\nabla p + \frac{\mu}{k}\underset{\sim}{v} + \rho\,\underset{\sim}{g} = 0 \tag{4.3}$$

The curl of eq. (4.3) is

$$\frac{\nabla\mu}{k} \times \underset{\sim}{v} - \frac{\mu}{k^2}\nabla k \times \underset{\sim}{v} + \frac{\mu}{k}\nabla \times \underset{\sim}{v} + \nabla\rho \times \underset{\sim}{g} = 0 \tag{4.4}$$

since $\nabla \times \nabla p = 0$. If the density and viscosity are functions of concentration, then

$$\nabla \times \underset{\sim}{v} = \left(\frac{\mu'}{\mu} v + \frac{\rho' k g}{\mu}\right) \times \nabla c + \nabla(\ell n\, k) \times \underset{\sim}{v} \tag{4.5}$$

where $\mu' = d\mu/dc$, $\rho' = d\rho/dc$, $\underset{\sim}{g}$ is the gravitational force vector, and $\underset{\sim}{v}$ is the Darcy velocity. In this form, the contribution of dispersion to the local velocity has been neglected as have variations in porosity. The more general case has also been considered by Heller (1966). If the flow is initially irrotational, as it is in uniform radial or linear displacements, then $\nabla \times \underset{\sim}{v} = 0$. It will remain so only if the vorticity, $\nabla \times \underset{\sim}{v}$, vanishes everywhere in the flow. If viscosity and density are independent of concentration, and if permeability does not vary, then each term in eq. (4.5) vanishes identically, and the flow will remain uniform. The flow may still remain uniform if there are no permeability variations and if the vector, $\mu'/\mu \, \underset{\sim}{v} + \rho' k/\mu \, \underset{\sim}{g}$, is aligned with the concentration gradient (Heller 1963, 1966). This will be true, for instance, in slow downward displacements of a viscous, dense fluid by a less viscous, less dense fluid. In that case, gravity forces stabilize an otherwise unstable displacement (Saffman & Taylor 1958; Dumoré 1964). Watkins (1978) used gravity segregation to stabilize displacements in CO_2 floods, where phase viscosities and densities are necessarily functions of composition. In the experiments reported below, we use fluids of closely matched density and viscosity to eliminate flow nonuniformities due to variations of fluid properties with composition.

The solution to eq. (4.2) for one set of boundary conditions has been given by Aronofsky and Heller (1957). Other boundary conditions have been considered by Aris and Amundson (1957), Brenner (1962), Coats and Smith (1964), and no doubt others. In practice, the solutions do not differ greatly except at early time in the inlet region, and even then, only when the Peclet number is small. The approximate solution

$$\frac{C}{C_o} = \frac{1}{2} \operatorname{erfc} \left\{ \frac{x - vt}{2\sqrt{Dt}} \right\} \qquad 0 \leq x \leq L \tag{4.6}$$

where C_o is the injected concentration (the concentration of i in the porous medium is assumed to be zero initially), and L is the system length, is usually used to determine the dispersion coefficient from effluent composition data (Brigham, Reed & Dew 1961; Perkins & Johnston 1963).

In the solution given in eq. (4.6), the midpoint of the transition zone moves with the displacement velocity v, and the composition profile is symmetric about the midpoint. In standard miscible displacement experiments, the composition profile at a fixed time cannot be observed. Instead, the compositions of fluids passing a fixed point, the core outlet, are measured. A plot of effluent compositions against time (or pore volumes injected) will be slightly asymmetric because the transition zone continues to grow during the time period during which it is produced. In actual displacements, however, observed effluent composition curves are often more asymmetric than can be explained by transition zone growth alone. At the trailing edge of the transition zone, the displaced fluid is recovered more slowly than predicted by eq. (4.6). Deans (1963) and Coats and Smith (1964) proposed models to account for the asymmetry. Both models hypothesized that some portion of the porous medium might be stagnant, so that fluid present in such "dead-end pores" would be recovered only by mass transfer into the flowing stream. Deans' model considered mass transfer from dead-end pores, but did not consider effects of longitudinal dispersion in the flowing stream. The model proposed by Coats and Smith accounted for both longitudinal dispersion and mass transfer from dead-end pores. Their model has the form

$$\begin{aligned} f \frac{\partial c}{\partial \tau} + (1 - f) \frac{\partial c^*}{\partial \tau} + \frac{\partial c}{\partial \xi} - \frac{1}{Pe} \frac{\partial^2 c}{\partial \xi^2} &= 0 \\ (1 - f) \frac{\partial c^*}{\partial \tau} &= a \, (c - c^*) \end{aligned} \tag{4.7}$$

where c is now the concentration in the flowing stream, f the flowing fraction, c* the concentration in the stagnant volume, $a = \phi KL/v$, and K the mass transfer coefficient. At its heart, the Coats-Smith model is an attempt to represent microscopic heterogeneity of the rock. It does so by using two additional parameters, the flowing fraction, f, and the dimensionless mass transfer coefficient, a, to describe the flow. Unfortunately, there is no simple way to measure f and a independently. Instead, the parameters are determined by history-matching effluent composition data.

Multi-variable curve fits of the type required to history match effluent composition data can be difficult to perform because the parameters may not be completely independent. For instance, if the flowing fraction, f, is near one, the calculated results are not sensitive to the value of the mass transfer coefficient, so that variation of a over large ranges may produce only small changes in the difference between the computed and experimental results. Examples of this sort of problem have been given by Stalkup (1970) and Batycky, Maini, and Fisher (1982). They point out that the effluent composition profile calculated for large values of a may be very close to that obtained for small values of a and large values of D. Thus, it may be difficult to determine parameters uniquely, especially when the experimental results also exhibit scatter.

Interpretations of miscible displacement experiments based on the Coats-Smith model have been reported for sandstones by Baker (1977); Batycky, Maini, and Fisher (1982); and Spence and Watkins (1980). Figs. 4.1 and 4.2 summarize dispersion and mass transfer coefficients reported for Berea sandstone cores. Even the dispersion coefficients (Fig. 4.1) show substantial scatter, though a trend of increasing D with increasing velocity is clearly evident. Mass transfer coefficients showed much more scatter, probably because the flowing fractions determined for the sandstone cores were close to one. In fact, Baker (1977) found the flowing fractions to be exactly one for the three displacements conducted in Berea cores and hence reported no mass transfer coefficients. Spence and Watkins (1980) reported flowing fractions ranging from 0.946 to 0.997 for sandstone cores, so again, mass transfer coefficients were probably only weakly determined. Batycky, Maini, and Fisher (1982) also found flowing fractions to be above 0.9 for a Berea core. While several authors have argued that the mass transfer coefficient probably depends on the flow velocity, the data in Fig. 4.2 provide little guidance as to the relationship.

Extensive miscible displacement data for carbonate cores have been reported by Baker (1977); Batycky, Maini, and Fisher (1982); and Spence and Watkins (1980). Dispersion coefficients determined using the Coats-Smith model are collected in Fig. 4.3. As for sandstones, a clear dependence on velocity is observed, though at any given velocity the range of coefficients is nearly two orders of magnitude, as might be expected given the variations in heterogeneity from core to core. Mass transfer coefficients for the carbonate cores are reported in Fig. 4.4. With some imagination, a velocity dependence can be discerned. Again, the range of values at a given velocity is large. While some of that variation is probably due to differences between cores, it must also reflect the lumping of a variety of physical mechanisms into a single mass transfer coefficient. In addition, the range may be partly due to differences in fitting procedures (Batycky, Maini & Fisher 1982).

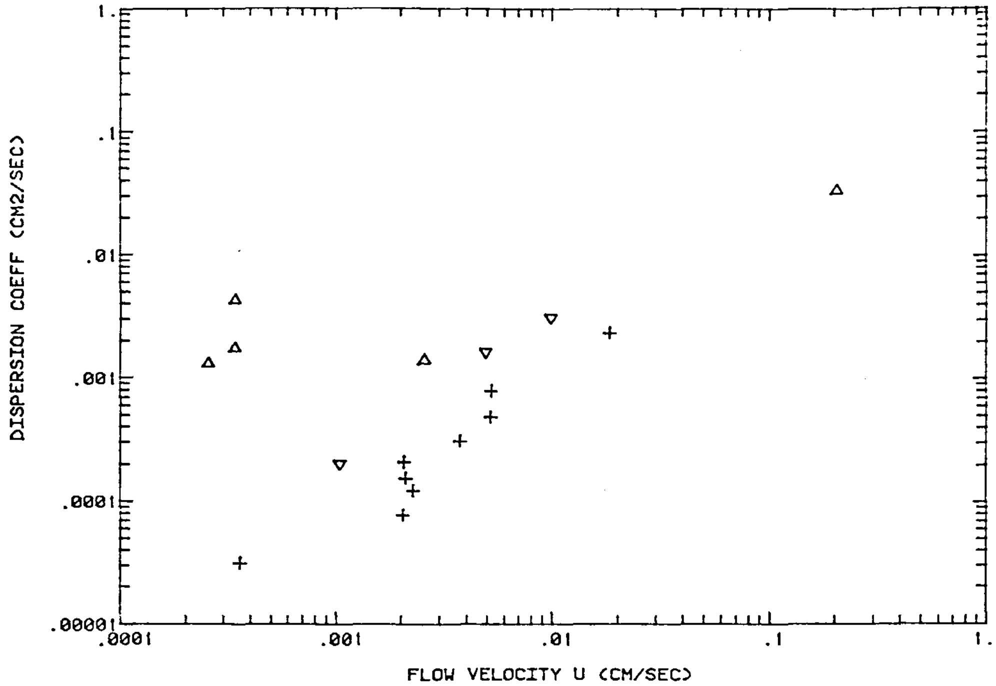

Fig. 4.1 Dependence of dispersion coefficients on flow velocity for sandstone samples. Sources of data: Δ Batycky, Maini, and Fisher (1982); + Spence and Watkins (1980); ∇ Baker (1977).

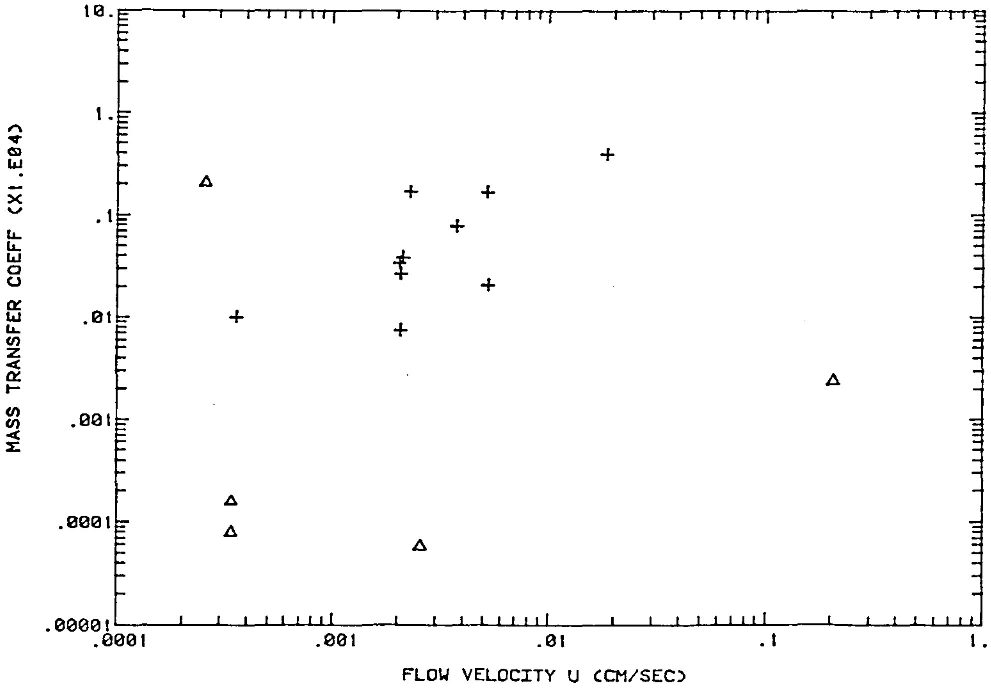

Fig. 4.2 Dependence of mass transfer coefficients on flow velocity for sandstone samples. Sources of data: Δ Batycky, Maini, and Fisher (1982); + Spence and Watkins (1980).

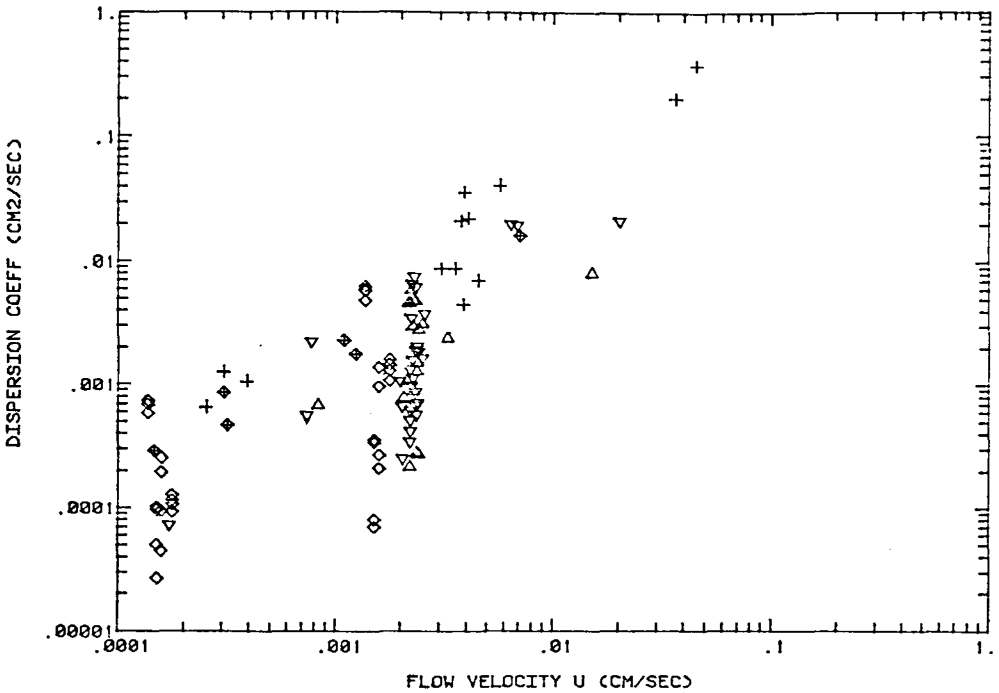

Fig. 4.3 Dependence of dispersion coefficients on flow velocity for carbonate core samples. Sources of data: + Batycky, Maini, and Fisher (1982); Δ Spence and Watkins (1980), carbonate A; ∇ Spence and Watkins (1980), carbonate B, ◇ Yellig and Baker (1980); ◈ Baker (1977).

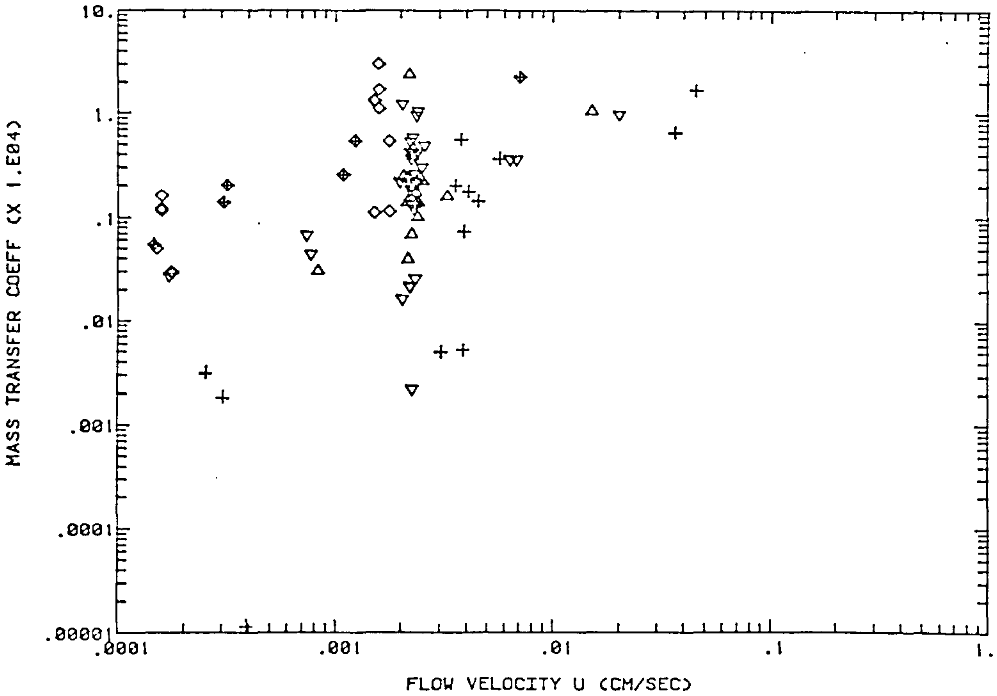

Fig. 4.4 Dependence of mass transfer coefficients on flow velocity for carbonate core samples. Sources of data: + Batycky, Maini, and Fisher (1982); Δ Spence and Watkins (1980), carbonate A; ∇ Spence and Watkins (1980), carbonate B, ◇ Yellig and Baker (1980); ◈ Baker (1977).

Flowing fractions determined for the various carbonate core samples are plotted against flow velocity in Fig. 4.5. Some, but by no means all, of the samples show much lower values of f than are typical for sandstones, but there is no clear dependence of f on flow velocity. Spence and Watkins (1980) argued that the flowing fraction was really a measure of local heterogeneity. In other words, the rock consists of some flow paths, presumably the larger pores, in which the flow velocity is greater than the overall average velocity and some flow paths in which flow is slower than the average. Thus, in the interpretation given by Spence and Watkins, it is not necessary that all of the fluid in the stagnant fraction of the pore volume be motionless, only that it move significantly more slowly than that in the flowing fraction. Analyses of pore size distributions for the cores studied supported their contention; samples with wider pore size distributions showed smaller values of f. Both Spence and Watkins (1980) and Batycky, Maini, and Fisher (1982) reported that for carbonate samples, f declined with increasing velocity. Such behavior is consistent with the idea that there exists a spectrum of flow velocities and that an increase in the displacement velocity increases the flow velocity more in the most permeable flow paths than in the slow flow paths. Thus, in the model interpretation, at high velocities the difference in velocity between slow and fast flow paths is larger and hence, more of the pore space is lumped into the class of slow moving or "stagnant" volume. Unfortunately, data reported so far do not appear to be sufficiently precise to test the hypothesis carefully. Fig. 4.6 reports only data for cores in which displacements were performed at more than one velocity. Those data, along with results of the replicated measurements reported by Yellig and Baker (1980) suggest that scatter in the flowing fraction, caused either by experimental error or by problems in fitting the results, is at least as large as any velocity effect.

Comparison of the results shown in Figs. 4.1 and 4.2 with those in Figs. 4.3-4.5 clearly indicates that miscible displacements are significantly less efficient in carbonate rocks. While questions remain about how the parameters obtained from the model proposed by Coats and Smith are related to the physical characteristics of the rocks and the fluids, that model is the only one in current use which attempts to account for effects of core heterogeneity on laboratory-scale displacements. Spence and Watkins presented convincing evidence that efficiency of both secondary and tertiary CO_2 floods in short cores correlates well with the measures of heterogeneity produced by the Coats-Smith model for miscible displacements in the same cores. Thus, the results of such model interpretations have some value as tools for characterization of laboratory core displacements.

Questions also remain about the impact of stagnant volumes on displacements at reservoir scale. Coats and Smith (1964) argued on dimensional grounds that the mass transfer group ($a = \phi KL/v$) is large at the displacement lengths and velocities typical of reservoir scales. A large mass transfer coefficient would lead to equalization of concentrations between flowing and nonflowing streams on a time scale which would be short compared to the time required for flow. Stalkup (1970); Spence and Watkins (1980); and Batycky, Maini, and Fisher (1982) used similar arguments and tested their scaling arguments in long core displacements. The experimental results supported the conclusion that mass transfer rate limitations are less

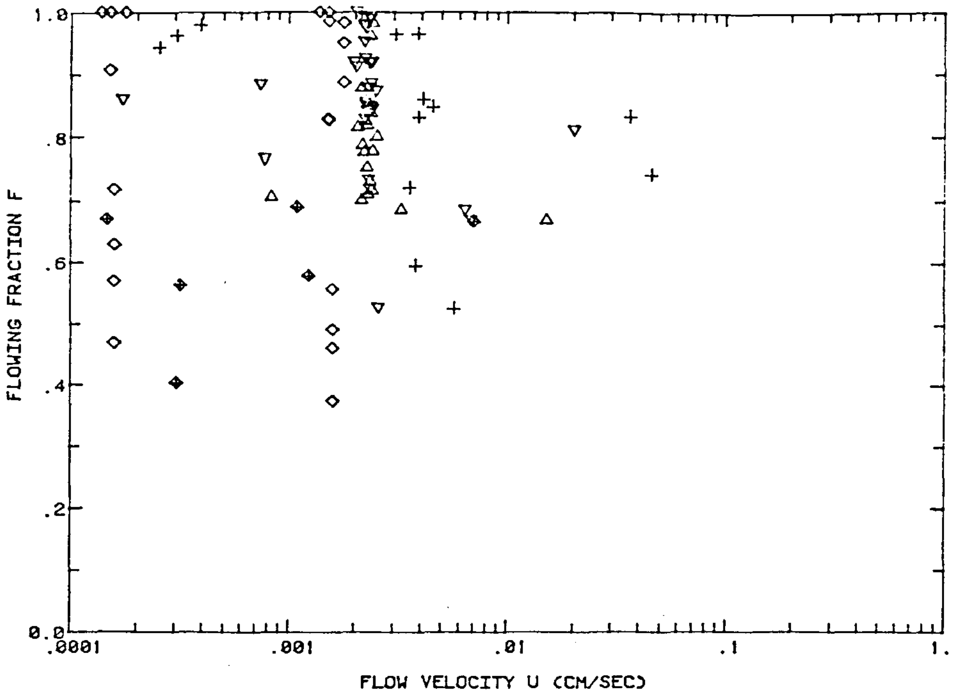

Fig. 4.5 Dependence of flowing fraction on flow velocity for carbonate core samples. Sources of data: + Batycky, Maini, and Fisher (1982); Δ Spence and Watkins (1980), carbonate A; ∇ Spence and Watkins (1980), carbonate B; ◇ Yellig and Baker (1980); ◈ Baker (1977).

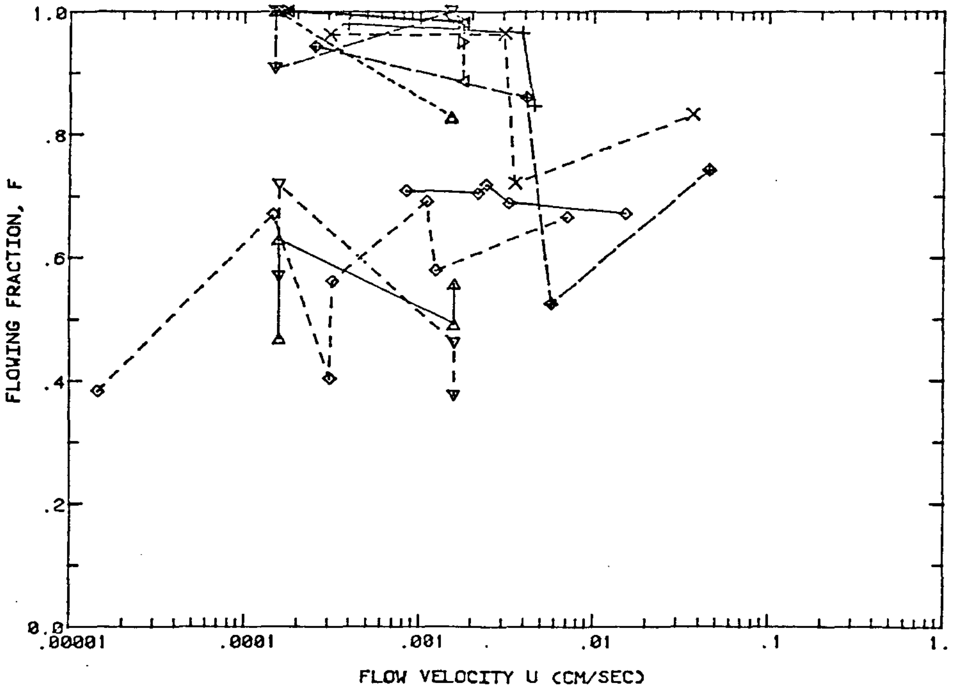

Fig. 4.6 Dependence of flowing fraction on flow velocity for carbonate core samples. Data shown are only those for which displacements were performed at different velocities in the same core. Sources of data: +——+, x---x, ◈———◈ Batycky, Maini, and Fisher (1982); ◇——◇ Spence and Watkins (1980); Δ-----Δ, ∇———∇, Δ——Δ, ∇- - -∇, ▷-----▷, ◁----◁ Yellig and Baker (1980); ◇----◇ Baker (1977).

important on a field scale. Baker's (1977) analysis of the effect of length differed, however. He derived an effective dispersion coefficient for long displacements which depended on the dimensionless group DK/u^2, but did not depend on length. In his approach, then, long displacements can be modeled by a simple dispersion model in which the apparent dispersion coefficient is larger than a local dispersion coefficient due to heterogeneity.

A fundamental assumption inherent in the arguments given by Coats and Smith (1964), Stalkup (1970), and Baker (1977) is that the dispersion and mass transfer coefficients remain constant as the scale of the displacements is increased. That assumption is probably not accurate. In real porous media, the dispersion and mass transfer coefficients measured inevitably include averaged effects of local heterogeneities (Heller 1963). For instance, dispersion coefficients measured on field scales are often several orders of magnitude larger than those determined on a laboratory scale, and quantitative estimates of the effects of heterogeneity on dispersion are available in the pioneering analysis of the impact of random variations on apparent dispersion coefficients by Gelhar, Gutjahr and Naff (1979). No such analysis of mass transfer from stagnant pore volume has been attempted, but it appears likely that a similar dependence on scale exists. Hence, it also appears likely that effects of mass transfer similar to those observed on a laboratory scale will occur on a field scale.

Two-Phase Displacements

Of particular interest for this study is the effect of high water saturations on the efficiency of CO_2 displacements. Effects of varying wetting phase saturation have been investigated by Raimondi, Torcaso and Henderson (1961); Thomas, Countryman and Fatt (1963); Raimondi and Torcaso (1964); Stalkup (1970); Shelton and Schneider (1975); Salter and Mohanty (1982); and Batycky, Maini, and Fisher (1982). In their first paper, Raimondi, Torcaso, and Henderson (1961) reported that while some oil was shielded by high water saturations, it could all be recovered eventually by continued miscible displacement. In their second paper (Raimondi & Torcaso 1964), however, they argued that the experiments reported previously were not conclusive since they had been performed with fluids for which the mobility ratio was adverse. In the second paper, they reported results of displacements of fluids with matched density and viscosity and found that significant fractions of hydrocarbons were permanently trapped. Their displacements were performed in Berea sandstone.

Thomas, Countryman, and Fatt (1963) reported evidence for what they called "dendritic pore volume" in the nonwetting phase caused by high wetting phase saturations, and reported that apparent dispersion coefficients determined for the nonwetting phase increased with increasing water saturation. They performed displacements in which paraffin was the wetting phase in Boise sandstone. The core was saturated with liquid paraffin, and then air was injected to establish a nonwetting phase saturation. The paraffin was solidified, and the pore space previously occupied by air was saturated with brine. Displacements of that brine by brine of a different sodium chloride concentration were used to investigate effects of a truly immobile "wetting" phase (solidified paraffin) on dispersive mixing in the "nonwetting" (water) phase. Thomas, Countryman, and Fatt (1963) argued on the basis of early breakthrough of the displacing fluid that some of the nonwetting phase was located in pores which did not contribute to the flowing stream, dead-end or dendritic pores whose shape was determined by the location of the wetting phase. They hypothesized that slow mass transfer out of the dendritic pores accounted for the broad transition zones they observed at high wetting phase saturations, and concluded that such flows could not be described adequately by a simple convection-dispersion model. The flow visualization experiments described in §3.3 confirmed that dendritic oil ganglia bounded by water do occur in porous media that contain no actual dead-end pores.

Stalkup (1970) interpreted miscible displacements of the oil phase at varying water saturations using the Coats-Smith model and found that the model did an adequate job of describing displacement of nonane (C_9) by undecane (C_{11}), but attempts to predict the displacement of C_9 by propane were much less successful. Stalkup argued that in an actual rock, there must be a spectrum of mass transfer coefficients and proposed a model in which two separate stagnant fractions were allowed to have different mass transfer coefficients. The new model did improve the fit to experimental results to some extent, but the agreement was still not as good as for the stable miscible displacements. It seems likely that the principal reason for the lack of agreement was that the displacements of C_9 by propane were unstable and probably dominated by viscous fingering. The Coats-Smith model does not attempt to account for the physics of finger growth, so it is not surprising that it does a poor job of predicting results of unstable displacements. Stalkup's results for stable, miscible displacements, however, clearly indicate that as water saturation increases, the flowing fraction decreases and apparent dispersion coefficient increases. Those observations are consistent with the idea that some of the oil present at a given water saturation resides in pores which may have more than one entrance or exit, but which are effectively dead-end because water blocks access of the flowing solvent stream to the trapped oil. Both effects indicate that, on a laboratory time scale at least, displacements of oil by CO_2 at high water saturations will be less efficient in rocks similar to the Berea sandstone used, which presumably was strongly water-wet. Examples of this sort of behavior were also observed in the experiments reported in §3.3.

Shelton and Schneider (1975) also used Berea cores to investigate effects of high water saturations. They suggested that at any given level of oil relative permeability, the difference in saturation between the primary drainage and imbibition oil relative permeability curves provides a measure of the trapped oil saturation. In addition, they argued that the wetting phase maintains continuous flow paths at all saturations and hence is not trapped and should be completely recoverable by solvent injection. In separate miscible displacements in the oil and water phases, they found that the presence of a second mobile phase slowed recovery of either phase, but the nonwetting phase recovery was much more strongly affected. All of the wetting phase could be recovered by a miscible displacement, but significant amounts of nonwetting phase remained unrecovered at the end of the tests, though oil was still being produced slowly. Those results suggest that oil recovery by solvent injection would be more efficient in oil-wet rocks. The tertiary CO_2-crude oil displacements described in §3.3 suggest that the presence of continuous oil-phase flow paths in fine pores and capillary grooves accounts for the more efficient recovery of the wetting phase.

Shelton and Schneider (1975) also compared secondary and tertiary miscible displacements for wetting and nonwetting phases. They found little difference between secondary and tertiary flood results. The floods were conducted, however, with adverse viscosity ratios in the neighborhood of 40:1, so that it is possible that viscous fingering dominated both sets of displacements. Transition zones were much longer than could be attributed to dispersion in both secondary and tertiary displacements, which suggests that effects of the distributions of phases on mixing may have been swamped by viscous fingering. Watkins (1978) successfully correlated residual oil saturations to CO_2 core floods with estimates of the importance of viscous fingering and suggested that the low recoveries observed by Shelton and Schneider at high displacement rates were a reflection of the effects of viscous fingering, and hence did not accurately measure the local displacement efficiency in the swept zone.

Tiffin and Yellig (1983) also investigated effects of wetting behavior in tertiary CO_2 floods in a Berea sandstone core. They performed CO_2 floods with water injected simultaneously. The core used for water-wet displacements was later treated to make it oil-wet. They found that preferential extraction of hydrocarbons from the oil still occurred in both water-wet and oil-wet displacements, but argued, based on visual observations of produced fluids, that simultaneous water injection caused significant amounts of oil to be isolated and interfered with the development of miscibility in the water-wet displacements. In displacements in oil-wet cores, oil recovery was higher and did not appear to be affected by simultaneous water injection.

Salter and Mohanty (1982) performed extensive two-phase, steady-state core floods in an acidized and fired Berea sandstone core. They investigated primary drainage, imbibition, and secondary drainage saturations. Miscible displacements in each phase were performed with matched viscosity fluids to eliminate the complications of flow instabilities. The recovery of the wetting phase was 100% in every case. Recovery of nonwetting phase varied with saturation and was less than 100% even after many pore volumes of fluids were injected. Effluent concentration histories for both phases were fit with the Coats-Smith model corrected for the unrecovered, trapped or isolated phase volume. For both wetting and nonwetting phases, the dispersion coefficient in the presence of the other phase was greater than the single-phase dispersion coefficient. Also, a significant dendritic volume appeared in both phases which was not present in the single-phase floods. Salter and Mohanty's results show that the presence of immiscible phases in a displacement increases the mixing or lengthens the transition zone for Berea sandstones, even when viscous instabilities are controlled. Further, some fraction of the nonwetting phase can be isolated from the flowing phase and is therefore unrecoverable with a solvent which is insoluble in the wetting phase.

The detailed examination of the behavior of flowing and trapped fractions, and dispersion and mass transfer coefficients as a function of water saturation reported by Salter and Mohanty (1982) for Berea sandstone is the most comprehensive reported to date for any rock sample. No such study has been reported for reservoir cores, however. Batycky, Maini and Fisher (1982) performed a limited number of displacements in carbonate cores containing immobile water saturations. They found that the presence of water did not change dispersion coefficients in the carbonate cores, but flowing fractions decreased with increasing water saturation. Mass transfer coefficients were higher for displacements with water present than for dry cores, but did not depend strongly on the magnitude of the water saturation. Effects of mobile water saturations in the carbonate cores were not examined.

Given the complexity of mixing phenomena in reservoir rocks, it can be difficult to interpret displacement experiments from effluent composition data, particularly when a process as complex as a multiple contact miscible CO_2 flood is also operating. For instance, viscous fingering, unfavorable phase behavior, and heterogeneity can all cause a broad transition zone, and hence, it can be difficult to sort out which mechanism or mechanisms dominate displacement efficiency. The experimental procedures described below are an attempt to eliminate the effects of viscous instability and the complications of CO_2-crude oil phase behavior, and thereby isolate the effects of core heterogeneity and screening of oil by high water saturations. Interactions of these mixing effects with phase behavior of CO_2-crude oil mixtures is examined in §5.3. It is clear, however, that quantitative interpretations of such experiments are still strongly dependent on the assumptions inherent in the model used to describe the flow, whether it be a dispersion model, a capacitance-dispersion model (Coats & Smith 1964) or some other approach. While there is no tractable alternative to describing complex flows in complicated porous media in terms of lumped parameters of some sort, the limitations inherent in that approach must be recognized.

4.2 Experimental Apparatus and Procedures

Both single-phase and two-phase, steady-state displacements were performed in reservoir core samples. The single-phase displacements were performed with fluids of matched density and viscosity and were intended to investigate effects of microscopic heterogeneity on displacement efficiency in an ideal miscible flood. The two-phase displacements, in which the oils of matched density and viscosity and brines with matched densities and viscosities different from the oils were used, were designed to study the effect of the presence of more than one phase in the pore space on mixing. Considerable effort went into the development of experimental equipment and techniques which would produce consistent results rapidly for small reservoir cores. Several versions of the equipment were tested. Described here are the current versions. For descriptions of earlier versions see Orr and Taber (1982, 1983).

Single-Phase Displacement Apparatus

Fig. 4.7 shows a schematic of the apparatus used for single-phase displacements. Injection of a slug (pulse) of displacing fluid is accomplished by a sample loop similar to those used for the injection of samples in gas and liquid chromatography. A sample loop of known volume was constructed from a coil of Teflon tubing. The experiment is performed by first filling the pump and core with one fluid and then loading the sample loop with a matching fluid. The pump is started at the proper displacement rate and the pressure drop across the core allowed to stabilize while the sample loop is in the by-pass configuration. Then the valve is switched to the "sample" position, which directs the flow from the pump through the loop before flowing to the core. The volume of the sample loop may be varied by using different lengths of tubing.

Compositions of produced fluids are monitored with a differential refractometer (Waters 401). Output from the refractometer is converted to digital form and is sampled periodically by the HP-85 microcomputer. Effluent from the refractometer is collected on a digital balance, also monitored by the HP-85 so that overall material balances and displacement rates can be checked.

In a typical displacement, the core is saturated with brine (2.0 wt. % NaCl, 1.0 wt. % $CaCl_2$, 0.01 wt. % NaN_3, saturated with $CaSO_4$, to which 0.4% sucrose is added). The brine in the pulse is the same as that used to saturate the core with the exception that the sucrose concentration is 0.52 wt. %. Sucrose was chosen as a tracer because it has minimal interaction with the rock surfaces and is not soluble in the oil phase that is present in two-phase displacements. In the concentration range used, it produces a linear response from the refractometer, as is shown in Fig. 4.8.

Single-phase displacements were also performed with other fluid pairs. In some early displacements, ethylbenzene and ethylbutyrate were used because they have closely matched density and viscosity at room temperature. In those experiments, effluent samples were collected and analyzed by gas chromatography. Ethylbenzene and ethylbutyrate were not used when effluent compositions were measured with a refractometer because mixtures of those components did not show linear detector response. Mixtures of decane and undecane did show linear response and were used for some displacements (see the discussion of two-phase displacements below). On-line conductivity measurements for brines containing differing amounts of NaCl were also used. While results of conductivity measurements were identical with those using hydrocarbons in Berea sandstone, unacceptable material balance errors resulted when conductivity measurements were used with carbonate cores. We speculate that leaching of minerals from the carbonate cores may have caused the problem. Thus, results of conductivity measurements are reported only for Berea sandstone. In all the displacement results reported below, the fluids and analytical method used are identified.

Cores were prepared for saturation with brine according to the following procedure:

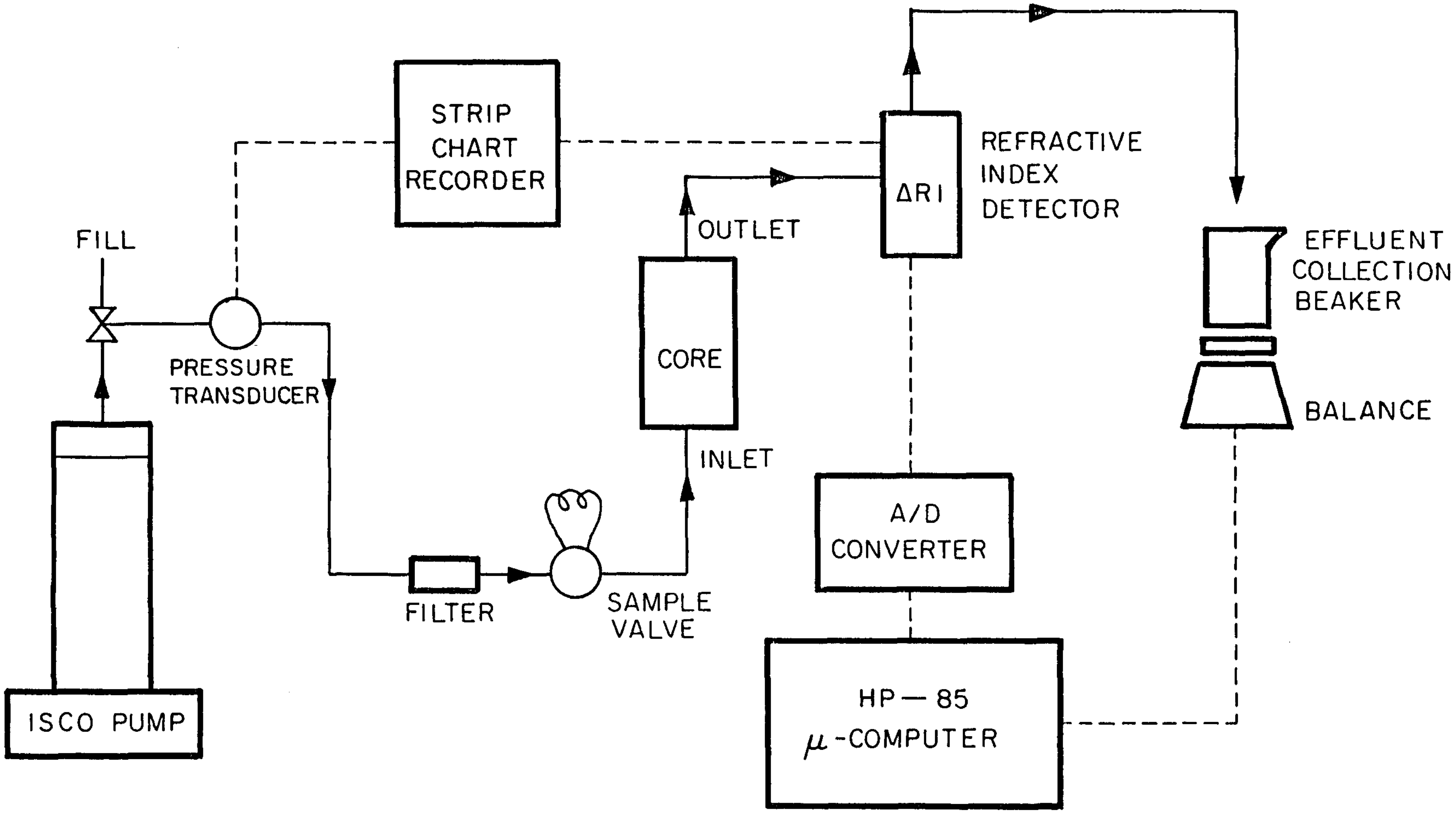
STRIP
CHART
RECORDER
FILL
PRESSURE
TRANSDUCER
ISCO PUMP
FILTER
SAMPLE
VALVE
CORE
OUTLET
INLET
ΔRI
REFRACTIVE
INDEX
DETECTOR
A/D
CONVERTER
HP — 85
μ-COMPUTER
EFFLUENT
COLLECTION
BEAKER
BALANCE

Fig. 4.7 Apparatus for single-phase displacements.

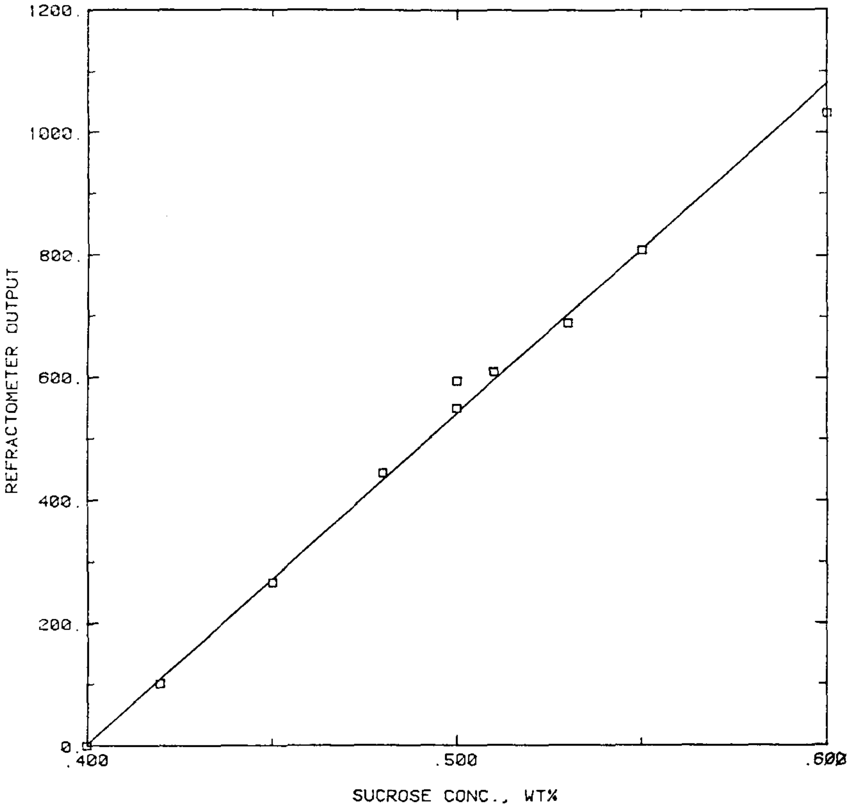

Fig. 4.8 Differential refractometer output for sucrose in brine. The brine contained 1 wt. % $CaCl_2$, 2 wt. % NaCl, $CaSO_4$ to saturate, and 0.1 wt. % NaN_3. The reference fluid was the same brine containing 0.4 wt. % sucrose.

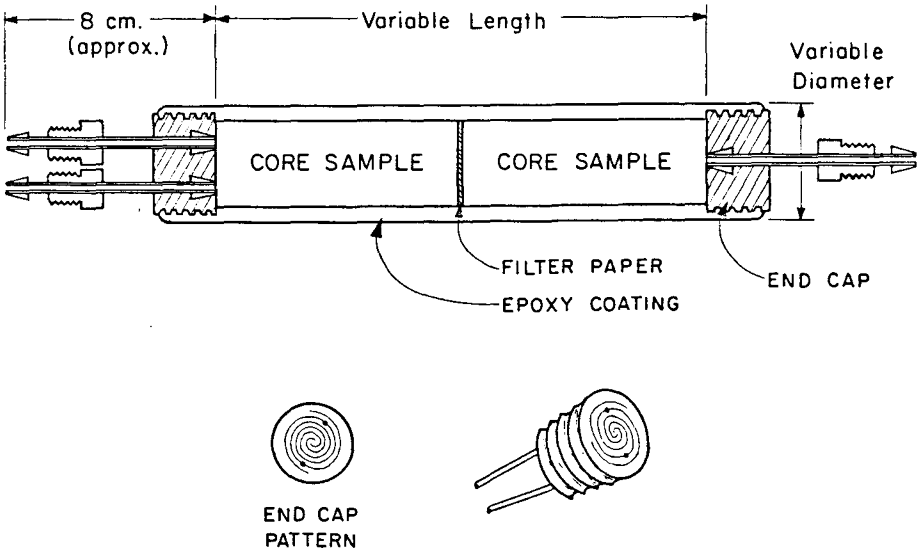
8 cm.
(approx.)
Variable Length
Variable
Diameter
CORE SAMPLE
CORE SAMPLE
FILTER PAPER
EPOXY COATING
END CAP
END CAP
PATTERN

Fig. 4.9 Core assembly.

(1) Horizontal cores (parallel to bedding plane) were cut to a diameter and length selected to give sufficient pore volume.

(2) The core was subjected to a lengthy Soxhlet extraction with a mixture of toluene and perchlorethylene.

(3) Cores were butted together separated by filter paper (Whatman #5) and end caps were mounted on the core faces. The core assembly was then coated with epoxy (Armstrong A661), and then wrapped with epoxy impregnated dacron tape (Fig. 4.9).

(4) Solvents (tetrahydrofuran, isopropanol and acetone) were displaced through the core.

(5) The core was dried, weighed, and air permeability was measured. It was then saturated with brine and weighed again to determine pore volume.

Fittings used were chosen to have minimum dead volume. Low dead-volume end caps were fabricated out of the same epoxy used to coat the core and were cast with a spiral groove on the face of the cap to distribute and collect fluids. The spiral was obtained by etching a glass plate by the same photographic technique used to make the micromodels described in §3.1. The spiral etched in glass was used to cast an epoxy negative with which the end cap was then cast.

A few of the single-phase displacements described in §4.4 were performed with hydrocarbons in place of brine. Hydrocarbon pairs used were ethylbenzene and ethylbutyrate, which also have closely matched density and viscosity (Orr & Taber 1982), and decane with undecane as a tracer. When ethylbenzene and ethylbutyrate were used, small samples were collected and analyzed by gas chromatography. Decane-undecane mixtures were analyzed on-line with the refractive index detector.

Two-Phase Displacement Apparatus

Upon completion of a series of single-phase miscible displacements at different velocities, the core is placed in the apparatus shown in Fig. 4.10. To establish connate water saturation, the brine-filled core is flooded with at least 100 pore volumes of decane. Finally, the core is flooded with at least 100 pore volumes of brine to establish the residual oil saturation. All saturations are determined by weight.

Once residual oil saturation is achieved, a secondary drainage, steady-state saturation of oil and water is established. Oil (decane) and water (brine) are pumped simultaneously at constant fractional flow through the core. When the pressure drop across the core remains constant for an appropriate time period (usually 24 hours), steady-state saturation is assumed to have been reached.

The 50 cc buret (Fig. 4.10) allows both fluids to be repeatedly

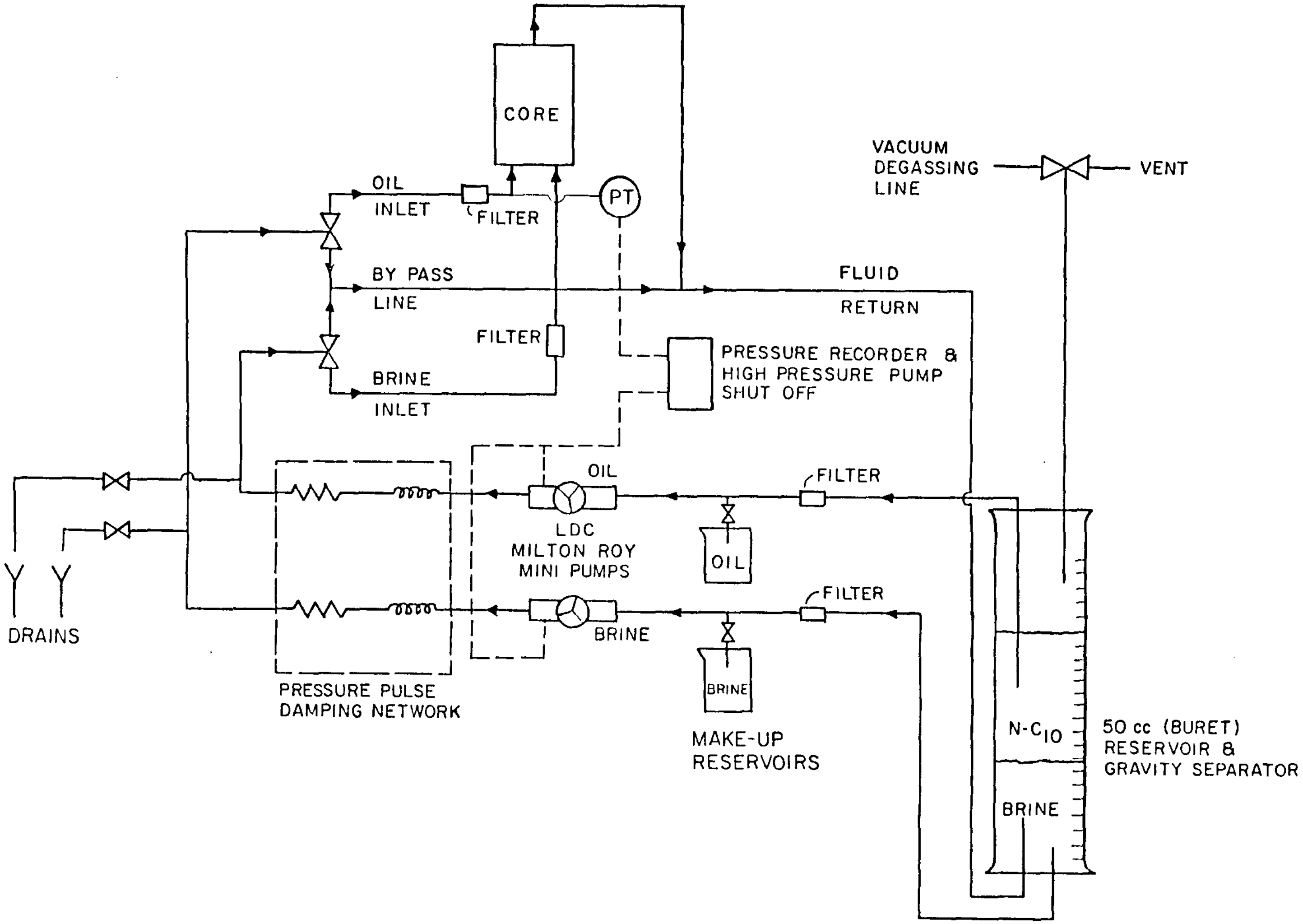
CORE
VACUUM DEGASSING LINE
VENT
OIL INLET
FILTER
PT
BY PASS LINE
FLUID RETURN
FILTER
PRESSURE RECORDER & HIGH PRESSURE PUMP SHUT OFF
BRINE INLET
OIL
FILTER
LDC MILTON ROY MINI PUMPS
OIL
FILTER
BRINE
BRINE
DRAINS
PRESSURE PULSE DAMPING NETWORK
MAKE-UP RESERVOIRS
N-C10
BRINE
50 cc (BURET) RESERVOIR & GRAVITY SEPARATOR

Fig. 4.10 Apparatus for saturation of a core with two phases.

circulated through the core without interrupting the operation nor requiring large volumes of oil and brine. The pulse damping network limits the size of the pulse to the core due to the positive displacement pumps. At a 300 psi core inlet pressure, the pressure oscillation is less than 5 psi.

Fig. 4.11 is a schematic of the apparatus used for two-phase displacement experiments. After the steady-state saturation has been established, the core is transferred to the two-phase displacement apparatus, which is similar to that used in single-phase displacements, except that both oil and brine displacements are conducted simultaneously. Both oil and brine of the same composition as the saturated core begin to flow through the core at the same fractional flow (but not necessarily the same total flow rate) used to establish the steady-state saturation. Since saturation is a function of fractional flow (if capillary end effects are small), there should be no redistribution of the phases, and the pressure drop across the core should establish itself and stabilize quickly. Once the pressure drop stabilizes, the flow from the pumps can be redirected through the sample valve, creating a step displacement of each phase. Step changes can be injected simultaneously or separately into the two phases.

Fluids leaving the core enter an on-line, continuous oil-water separator (Bretz, Pelletier & Orr 1984). Fig. 4.12 is a schematic of that device. The two-phase fluid enters a chamber in a disk-shaped, horizontal space between two porous membranes which have different wetting behavior. Oil, the less dense phase, rises and contacts the upper, hydrophobic membrane. Water settles and contacts the lower, water-wet membrane. (Membranes used in this study were obtained from Gelman Sciences, Inc., Ann Arbor, MI.)

Because it is hydrophobic, the upper membrane will resist passing water through its pores but will readily admit the nonpolar oil. The lower membrane can be wet by either oil or water, but if first wet by water, surface tension effects will prevent oil from entering the pores. Therefore, the first step in operating the separator is to prime it with water to establish a water-wet condition which must be maintained during operation.

Prior to assembly of the separator, the water-wet membrane is saturated using a vacuum to eliminate air from the pore spaces. After assembly, the separator is filled with water to the level of the vent of the siphon-breaker. Without the siphon-breaker, the weight of the water column extending below the separator will tend to pull air into the separator, possibly causing a loss of the water-wet condition. With the siphon-breaker, a few inches of positive water-head can be imposed on the water-wet membrane at all times, thus helping to maintain the water-wet condition.

Because a flowing stream of oil and water can be separated continuously in the mixing chamber with small volume (about 0.3 cm^3), it is possible to measure the composition of each phase continuously and on-line. The separated oil and water phases pass through refractometers, where compositions are measured, and then are collected on digital balances so that material balances and rates can be checked.

Brine with sucrose as a tracer is used for the water phase as in the

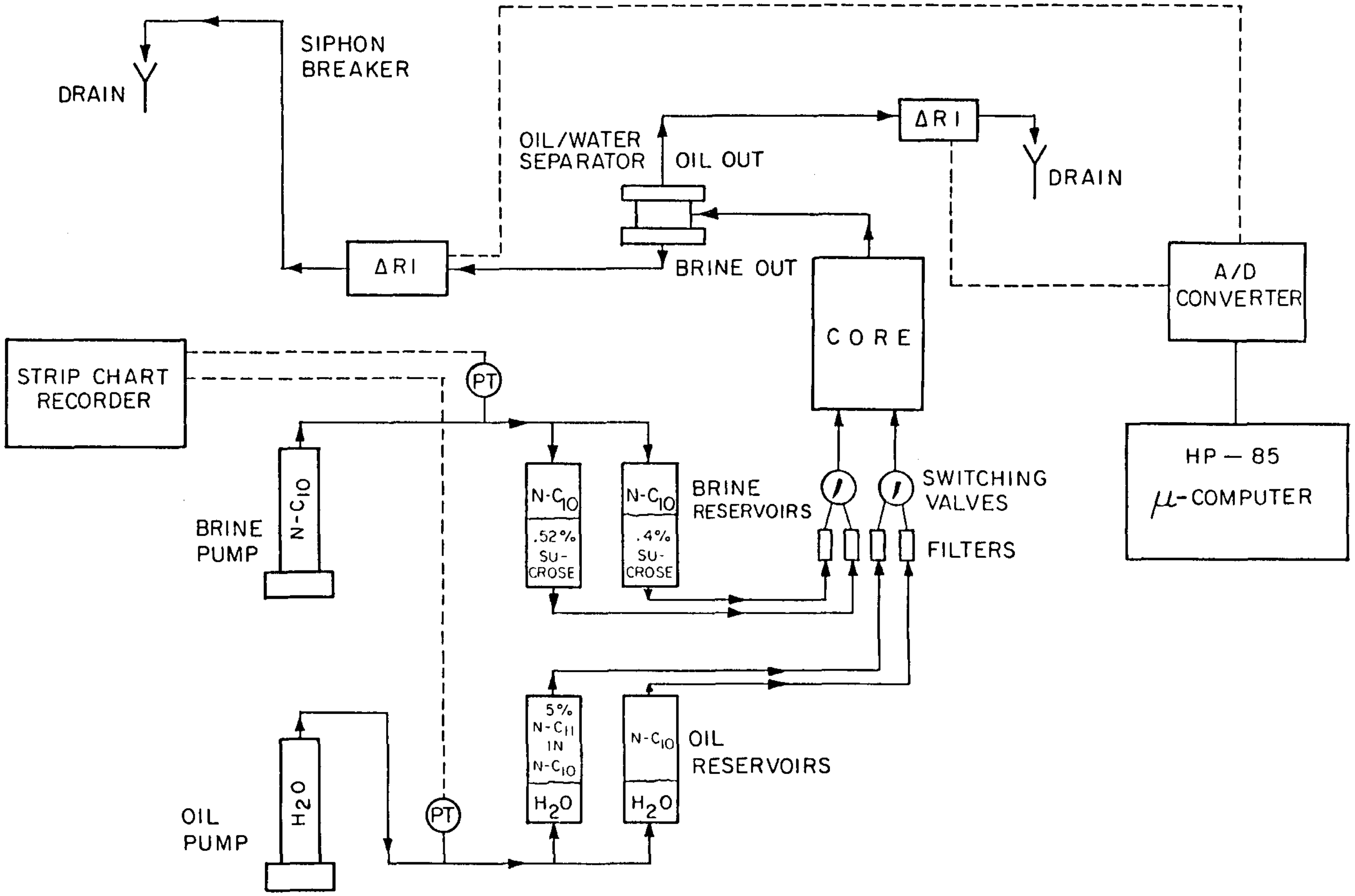
DRAIN
SIPHON BREAKER
ΔRI
OIL/WATER SEPARATOR
OIL OUT
BRINE OUT
ΔRI
DRAIN
CORE
A/D CONVERTER
HP — 85
μ-COMPUTER
STRIP CHART RECORDER
PT
BRINE PUMP
N-C_{10}
N-C_{10}
.52% SU-CROSE
N-C_{10}
.4% SU-CROSE
BRINE RESERVOIRS
SWITCHING VALVES
FILTERS
OIL PUMP
H_2O
PT
5% N-C_{11} IN N-C_{10}
H_2O
N-C_{10}
H_2O
OIL RESERVOIRS

CO_2-83-155

Fig. 4.11 Apparatus for steady-state, two-phase displacements.

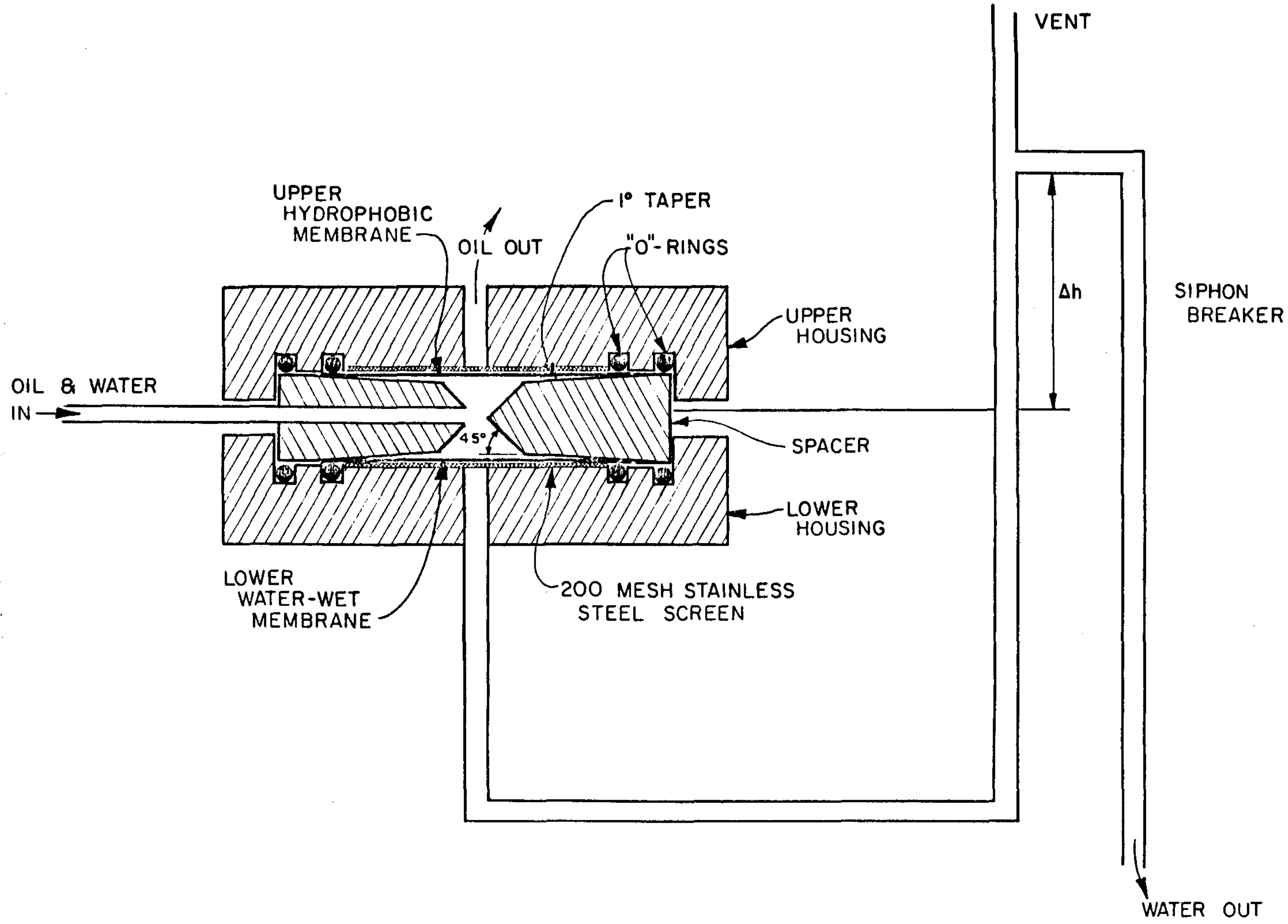
VENT
UPPER HYDROPHOBIC MEMBRANE
OIL OUT
1° TAPER
"O"-RINGS
Δh
SIPHON BREAKER
UPPER HOUSING
OIL & WATER IN
45°
SPACER
LOWER HOUSING
LOWER WATER-WET MEMBRANE
200 MESH STAINLESS STEEL SCREEN
WATER OUT

Fig. 4.12 Low dead volume oil-water separator.